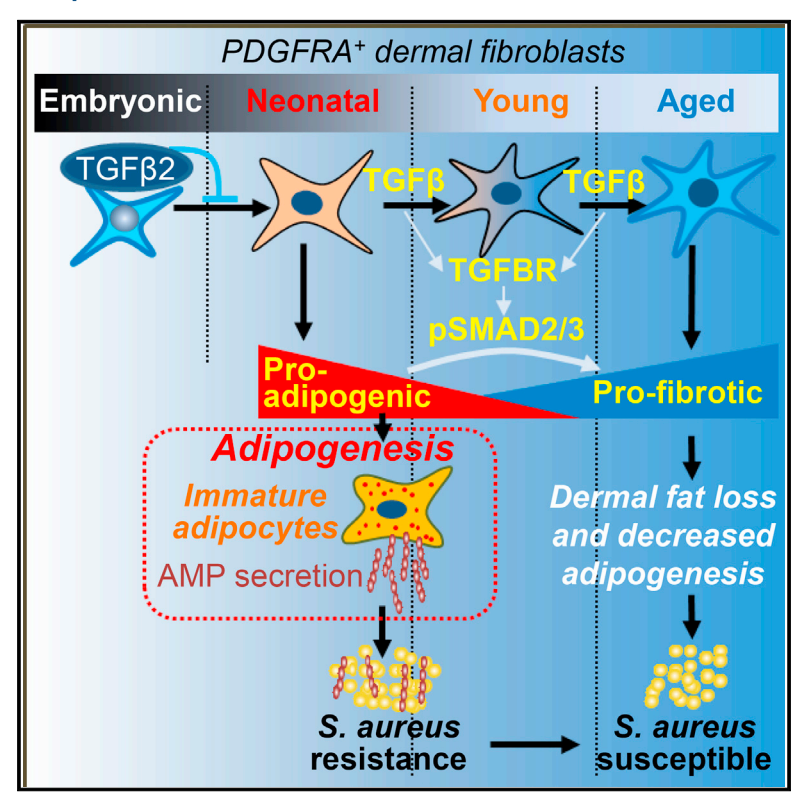
Immunity

Age-Related Loss of Innate Immune Antimicrobial Function of Dermal Fat Is Mediated by Transforming Growth Factor Beta

Graphical Abstract



Authors

Ling-juan Zhang, Stella Xiang Chen, Christian F. Guerrero-Juarez, ..., Ye Zheng, Maksim V. Plikus, Richard L. Gallo

Correspondence

lingjuan.zhang@xmu.edu.cn (L.-j.Z.), rgallo@ucsd.edu (R.L.G.)

In Brief

Dermal immature adipocytes fight against *Staphylococcus aureus* infection by secreting antimicrobial peptides during adipogenesis. Zhang et al. demonstrate that activation of the TGF-β pathway suppresses the adipogenic potential of dermal fibroblasts and therefore leads to an age-dependent loss of antimicrobial protection from dermal fat.

Highlights

- Neonatal skin is enriched with immature fat and adipogenic dermal fibroblasts
- Dermal immature fat and adipogenic-antimicrobial dFBs are lost with age
- TGF-β pathway promotes the age-related adipogenic-tofibrotic switch of dFBs
- Inhibition of TGFBR restores antimicrobial function of dFBs in adult mice







Age-Related Loss of Innate Immune Antimicrobial Function of Dermal Fat Is Mediated by Transforming Growth Factor Beta

Ling-juan Zhang,^{1,2,*} Stella Xiang Chen,² Christian F. Guerrero-Juarez,^{3,4} Fengwu Li,² Yun Tong,² Yuqiong Liang,⁶ Marc Liggins,² Xu Chen,⁵ Hao Chen,⁵ Min Li,⁵ Tissa Hata,² Ye Zheng,⁶ Maksim V. Plikus,^{3,4} and Richard L. Gallo^{2,7,*}

SUMMARY

Dermal fibroblasts (dFBs) resist infection by locally differentiating into adipocytes and producing cathelicidin antimicrobial peptide in response to Staphylococcus aureus (S. aureus). Here, we show that neonatal skin was enriched with adipogenic dFBs and immature dermal fat that highly expressed cathelicidin. The pool of adipogenic and antimicrobial dFBs declined after birth, leading to an age-dependent loss of dermal fat and a decrease in adipogenesis and cathelidicin production in response to infection. Transforming growth factor beta (TGF-β), which acted on uncommitted embryonic and adult dFBs and inhibited their adipogenic and antimicrobial function, was identified as a key upstream regulator of this process. Furthermore, inhibition of the TGF-β receptor restored the adipogenic and antimicrobial function of dFBs in culture and increased resistance of adult mice to S. aureus infection. These results provide insight into changes that occur in the skin innate immune system between the perinatal and adult periods of life.

INTRODUCTION

Staphylococcus aureus (S. aureus) is responsible for the majority of skin and soft-tissue infections in humans, and MRSA (methicillin-resistant S. aureus) infections over the past two decades were responsible for more deaths in the United States than any other pathogen (Klein et al., 2007; Miller and Cho, 2011). It is difficult to treat S. aureus infections because of its evolved resistance to common antibiotics; therefore, a better understanding of skin host defense mechanisms against S. aureus is acutely

needed for developing strategies to combat this important public health problem.

Skin provides a physical and immunological barrier protecting internal tissues from external insults. Dermal white adipose tissue (dWAT) is the deepest barrier of the skin and an understudied fat depot compared with inguinal white adipose tissue (iWAT) and epididymal white adipose tissue (eWAT) (Zwick et al., 2018). Until recently, dWAT was thought to function merely as an energy reservoir and a thermo-insulating layer. Recent studies, however, have revealed that dWAT also plays active roles in various physiological and pathological processes, such as the regeneration of hair follicles (Festa et al., 2011), wound healing (Plikus et al., 2017; Schmidt and Horsley, 2013), thermogenesis (Kasza et al., 2014), skin fibrosis (Marangoni et al., 2015), and protection against skin infection (Zhang et al., 2015). dWAT is produced by a subpopulation of dermal fibroblasts (dFBs). dFBs are a major skin cell type that has considerable functional diversity (Philippeos et al., 2018; Tabib et al., 2018). The reticular dermis contains dFBs with adipocyte progenitor properties, and these cells can commit to preadipocytes (pAds) and differentiate into adipocytes (ADs) upon stimulation (Driskell et al., 2013; Festa et al., 2011; Schmidt and Horsley, 2013; Zhang et al., 2015).

S. aureus skin infection triggers the rapid and localized differentiation of pAds to ADs, and we refer to this process as reactive adipogenesis. Reactive adipogenesis is characterized by the proliferation of adipocyte progenitor cells expressing preadipocyte factor 1 (PREF1) and is followed by their differentiation into immature ADs (Zhang et al., 2015). During this process, cathelicidin antimicrobial peptide (Camp) is abundantly expressed during the immature AD stage of differentiation. This expression of Camp is necessary to limit bacterial spread because the inhibition of this adipogenic-antimicrobial function of immature ADs leads to increased susceptibility to S. aureus infection (Zhang et al., 2015).

In this study, we sought to better understand the regulation of reactive adipogenesis in skin innate immunity. To explore this



¹School of Pharmaceutical Sciences, Xiamen University, Xiamen, China

²Department of Dermatology, University of California, San Diego, La Jolla, CA 92093, USA

³Department of Developmental and Cell Biology, Sue and Bill Gross Stem Cell Research Center, University of California, Irvine, Irvine, CA 92697, USA

⁴Center for Complex Biological Systems, University of California, Irvine, Irvine, CA 92697, USA

⁵Institute of Dermatology, Jiangsu Key Laboratory of Molecular Biology for Skin Diseases and STIs, Chinese Academy of Medical Science and Peking Union Medical College, Nanjing 210042, China

⁶Nomis Foundation Laboratories for Immunobiology and Microbial Pathogenesis, Salk Institute for Biological Studies, La Jolla, CA 92037, USA

⁷Lead Contact

^{*}Correspondence: lingjuan.zhang@xmu.edu.cn (L.-j.Z.), rgallo@ucsd.edu (R.L.G.) https://doi.org/10.1016/j.immuni.2018.11.003

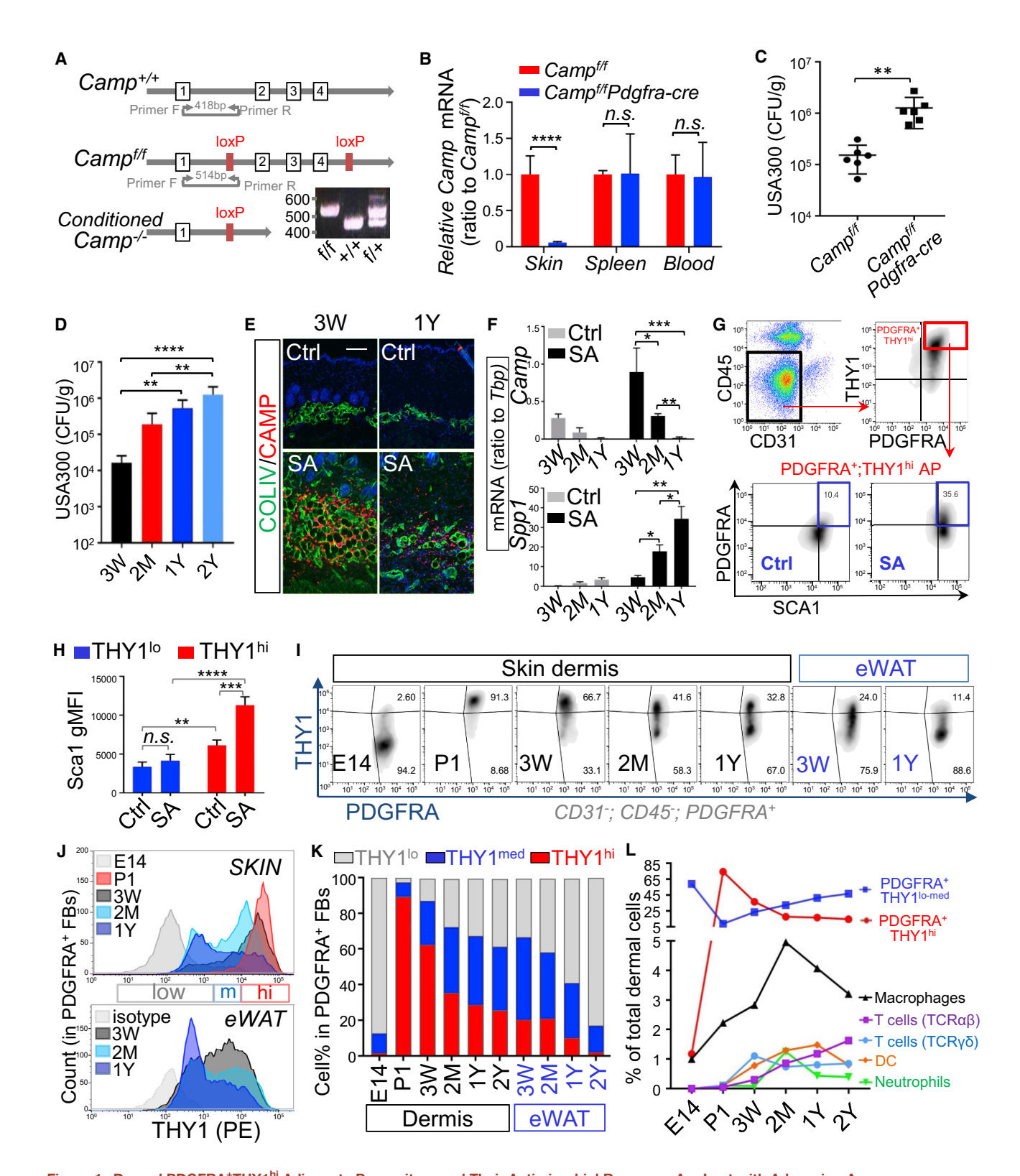


Figure 1. Dermal PDGFRA⁺THY1^{hi} Adipocyte Progenitors and Their Antimicrobial Response Are Lost with Advancing Age

(A) Schematic representation of the mouse *Camp* locus with exons 2–4 flanked by LoxP sites. The inset gel image represents the genotyping result of WT (+/+), heterozygote (f/+), and homozygous mutant (f/f) mice by using primers flanking *Camp* as indicated.

(B) *Camp*^{t/f} (WT) or *Camp*^{t/f} (Pdgfra-cre (Camp^{t/f}; Pdgfra-cre) littermate mice (2 months of age) were infected intradermally (i.d.) with *S. aureus*, and *Camp* mRNA expression (ratio to housekeeping gene *Tbp*) in skin or spleen tissues was measured by qRT-PCR analyses (n = 3–5 per group).

(C) Measurement of bacterial CFU from the infection edge area of the skin from infected $Camp^{t/t}$ or $Camp^{t/t}$ Pdgfra-cre mice (n = 6 per group).

question, we investigated changes in adipogenic function of dFBs during embryonic and adult development in mouse and human skin. A decrease in the capacity of dFBs to differentiate into adipocytes and express cathelicidin was observed to occur after birth and during the adult period of life. Furthermore, transforming growth factor beta (TGF- β) was identified to induce the loss of adipogenic potential and antimicrobial function of dFBs. These results uncover a previously unknown mechanism that impairs innate immune defense of the skin.

RESULTS

Dermal PDGFRA⁺THY1^{hi} Adipocyte Progenitors and Their Antimicrobial Response Are Lost with Advancing Age

To establish the contribution of adipocyte-lineage cells compared with non-adipocyte-lineage cells to cathelicidin expression, we generated mice to permit conditional deletion of Camp by inserting LoxP sites flanking exons 2-4 (Figure 1A). We crossed these Camp flox/flox mice with Pdgfra-cre or Adipoq-cre mice to delete Camp in dFBs that express Pdgfra (Campf/fPdgfra-cre) or cells that express Adipoq (Campf/f Adipoq-cre) in the later pAD stage. Flow cytometry and qRT-PCR validated that *Pdgfra* or *cre* expression was highly enriched in THY1⁺CD45⁻ dFBs, but not in THY1⁻CD45⁺ myeloid immune cells or spleen tissue (Figures S1A and S1B). Upon S. aureus infection, Camp expression was significantly suppressed in the Camp^{f/f}Pdgfra-cre and Camp^{f/f}Adipoq-cre skin, but not in the spleen or blood cells (Figures 1B and S1C-S1E). Camp^{f/f} Pdgfra-cre and Campff Adipog-cre mice became significantly more susceptible to S. aureus infection than wild-type (WT) littermate controls (Figures 1C and S1F-S1H). These results reinforce the conclusion that cathelicidin derived from cells of the adipocyte lineage plays a role in defense against S. aureus infection.

In general, innate immune defense is maximal in late fetal and early postnatal life and declines with age (Futata et al., 2012; Georgountzou and Papadopoulos, 2017; Shaw et al., 2013). An age-dependent decrease in the ability of skin to clear bacteria was evident by increased bacterial colony-forming units (CFU) in the infection edge area with advancing age (Figures 1D and S1I). To understand the contribution of adipogenesis to this loss of innate immune defense, we next examined the expression of cathelicidin in the cells of the adipocyte lineage during ag-

ing. A progressive loss of the capacity of *S. aureus* to trigger reactive adipogenesis was observed with advancing age, as measured by lesser staining of cathelicidin (Figure 1E) and lower expression of *Pref1* and *Camp* mRNA (Figures S1J and 1F) in dWAT at sites of infection. Loss of dermal reactive adipogenesis in response to *S. aureus* correlated with an age-dependent increase in the mRNA expression of *Spp1*, a pro-fibrotic marker (Figure 1F).

Next, we established a flow-cytometry method to define dFB cell populations that are activated upon S. aureus infection. Adipogenic dFBs were gated as CD31-;CD45-;PDGFRA+;THY1hi cells (Chia et al., 2016; Rivera-Gonzalez et al., 2016). S. aureus infection triggered an increase in surface expression of PDGFRA and Sca1 in THY1hi;PDGFRA+ cells, but not in THY1lo;PDGFRA+ cells (Figures 1G, 1H, and S1K). This suggested that reactive adipogenesis was restricted to THY1hi dFBs. To determine whether age-related loss of reactive adipogenesis was associated with the loss of THY1hi dFBs, we analyzed THY1 expression in PDGFRA⁺ dFBs in the late embryos and in mice up to 2 years of age. Fibroblasts from eWAT were also analyzed because eWAT has been previously reported to have age-associated dysfunction in adipogenesis and increased production of pro-inflammatory cytokines and fibrotic features (Kirkland et al., 1993; Sun et al., 2013). Flow-cytometry analyses revealed that PDGFRA+ fibroblasts in eWAT progressively lost THY1 expression with advancing age (from 3 weeks, 2 months, and 1 year to 2 years old), and by 1-2 years of age, PDGFRA+ fibroblasts in eWAT were mostly THY110 (Figures 1I-1K). In the skin, embryonic day 14 (E14) PDGFRA+ dFBs were mostly THY1lo (>97%) and became mostly THY1^{hi} (>90%) by postnatal day 1 (P1). Similar to that in eWAT, THY1 expression in dermal PDGFRA+ fibroblasts then became progressively lost during postnatal development and aging (Figures 1I-1K). Thus, age-related loss of THY1 expression is a common feature of PDGFRA+ fibroblasts in both eWAT and skin.

Next, age-related changes in PDGFRA+ dFBs were evaluated in parallel with changes in myeloid- or lymphoid-derived immune cells, including CD11B+F4/80+ macrophages, CD11B+Ly6Ghi neutrophils, CD11C+F4/80- dendritic cells (DCs), CD45+ T cell receptor (TCR) $\gamma\delta^+$ T cells and CD45+TCR $\alpha\beta^+$ T cells (Figures 1L, S1M, and S1N). PDGFRA+THY1hi dFBs represented the major resident innate cell type ($\sim\!75\%$ of total dermal cells) in neonatal (P1) skin. During postnatal development (at 3 weeks

⁽D) 3-week-old, 2-month-old, 1-year-old, or 2-year-old WT mice were infected i.d. with S. aureus, and bacteria CFU count was measured from the infection edge area (n = 4-5 per group).

⁽E) Cathelicidin (red) and COLIV (green) immunohistochemistry staining in control or S. aureus-infected skin (representative of n=3 per group). Nuclei were stained with DAPI (blue). Scale bars, 100 μ m.

⁽F) qRT-PCR of Camp or Spp1 expression in S. aureus-infected skin or control skin (ratio to Tbp) (n = 3-5 per group).

⁽G) Flow-cytometry plots for gating strategies for dermal PDGFRA+THY1hi adipocyte progenitors (representative of n = 3 per group).

⁽H) Flow-cytometry quantification of the geometric mean fluorescence intensity (gMFI) of Sca1 expression in THY1^{lo} or THY1^{lo} CD31⁻CD45⁻PDGFRA⁺ dFBs in control or *S. aureus*-infected skin (n = 3 per group).

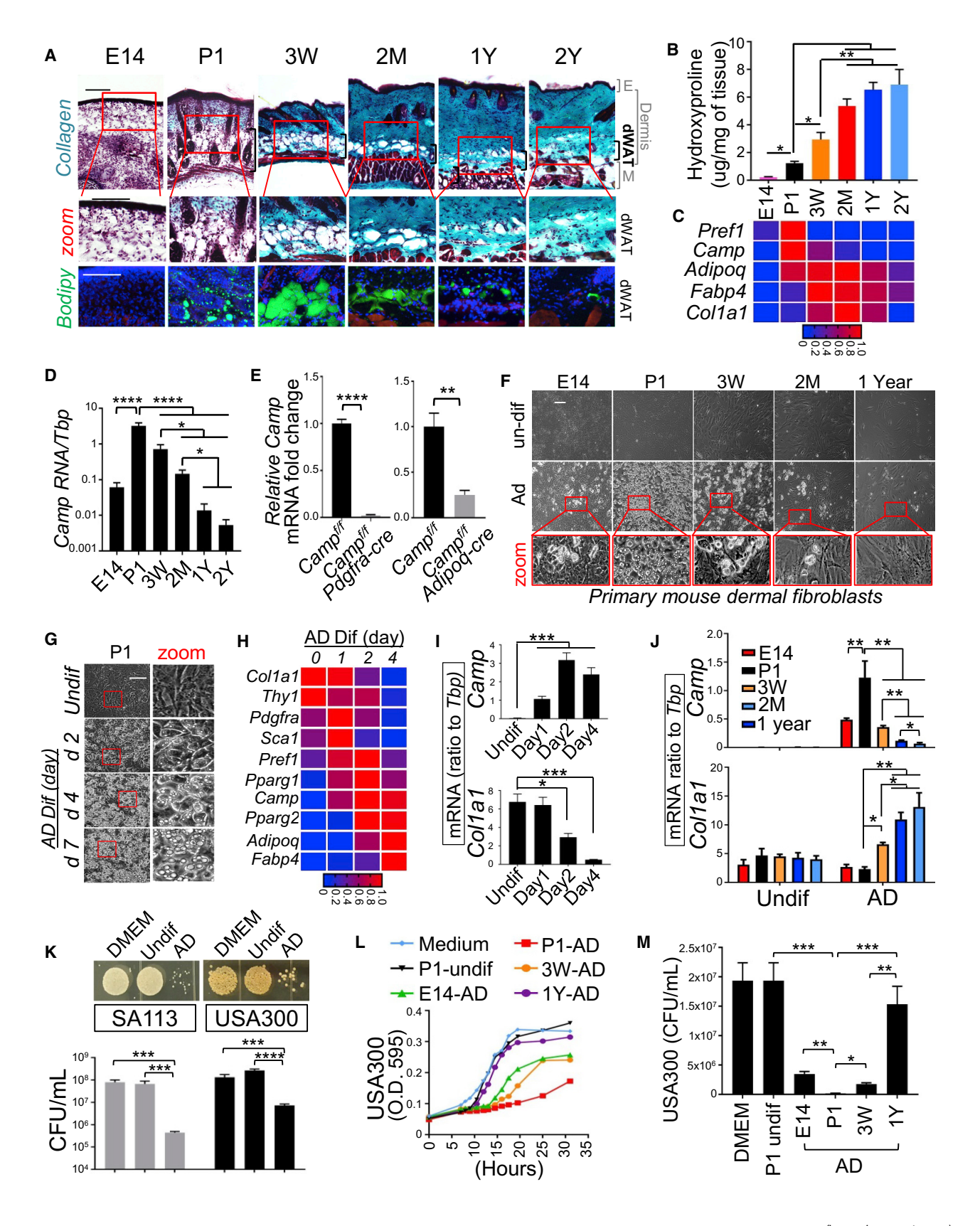
⁽I) Flow-cytometry plots of THY1 and PDGFRA in CD31 $^-$ CD45 $^-$ PDGFRA $^+$ FBs in skin dermis or eWAT (representative of n = 3 per group).

⁽J) Overlaid histogram of THY1 expression in CD31 CD45-PDGFRA+ FBs in skin dermis or eWAT (representative of n = 3 per group).

⁽K) Stacked bar graphs showing age-dependent changes of the percentage of THY1^{lo}, THY1^{med}, and THY1^{hi} cells in CD31⁻CD45-PDGFRA⁺ FBs in skin dermis or eWAT (average of n = 3 per group).

⁽L) Age-dependent changes of the percentage of THY1^{lo-med}PDGFRA⁺ fibroblasts, THY1^{hi}PDGFRA⁺ fibroblasts, CD11B⁺F4/80⁺ macrophages, CD11B⁺Ly6G⁺ neutrophils, CD11C⁺F4/80⁻ dendritic cells, CD45⁺TCR $\gamma\delta$ ⁺ T cells, and CD45⁺TCR $\alpha\beta$ ⁺ T cells in the total dermal cell population as indicated (average of n = 3 per group).

All error bars indicate mean ± SEM. *p < 0.05, **p < 0.01, ***p < 0.001 (one-way ANOVA). Please also see Figure S1.



(legend on next page)

and 2 months of age), the decline in THY1^{hi} dFBs was accompanied by an increase in myeloid-derived immune cell populations. Upon aging (at 1 or 2 years of age), the THY1^{hi} dFB population continued to decline, as did macrophages and DCs, whereas CD45⁺TCR $\alpha\beta$ ⁺ cells increased both in the skin and in eWAT (Figures 1L, S1M, and S1N).

Next, we characterized whether age-related changes in adipogenic dFBs correlated with changes in dermal fibrogenesis and adipogenesis. As shown in Figure 2A, whereas dWAT and the fibrogenic features (collagen staining and dermal hydroproline content) of the dermis were not developed in E14 skin, neonatal skin featured a large volume of dWAT with immature adipocytes and numerous small lipid droplets (Figures 2A, 2B, and S2A). Dermal adipocytes matured (indicated by large lipid droplets) by 3 weeks of age and were then gradually lost during adulthood and aging (from 2 months to 2 years of age) (Figure 2A). Loss of immature dermal fat with advancing age was also supported by an early peak at P1 in the mRNA expression of Pref1 and Camp, genes associated with early adipogenesis, and their subsequent progressive decline from postnatal development through aging (Figures 2C and 2D). Immunostaining for cathelicidin confirmed that it was abundantly expressed by P1 immature dermal ADs, whereas its expression was decreased in mature 3-week-old ADs and became undetectable in the 1-year-old ADs (Figure S2B). Deletion of Camp in Pdgfra+ dFBs (Camp^{f/f}Pdgfracre) or Adipoq⁺ ADs (Camp^{f/f}Adipoq-cre) led to a >95% and ~75% reduction in Camp mRNA expression in neonatal skin, respectively (Figure 2E), confirming that differentiating immature ADs are the major cellular source of cathelicidin in neonatal skin. The expression of mature adipocyte markers, including Adipog and Fabp4, peaked from 3 weeks to 2 months of age and then decreased progressively from 2 months to 2 years of age (Figures 2C and S2C), supporting our histological observation that mature ADs were lost with age. Age-dependent loss of immature dermal fat coincided with an age-dependent gain in dermal fibrotic features, especially in the dWAT layer, as shown by collagen staining, hydroxyproline measurement, and Col1a1 mRNA expression (Figures 2A-2C and S2D). Elastic fibers in dFBs also developed postnatally, and they became less dense in the lower dermis with advancing age (Figure S2A). By 2 years of age, the dermis appeared thinner and Col1a1 mRNA expression was low (Figures 2A and S2D), and the dWAT layer became devoid of ADs and showed extensive collagen staining (Figures 2A and S2A). Altogether, these results show that age-dependent loss of adipogenic dFBs is associated with a progressive loss of immature dermal fat and gain of fibrotic features.

To define adipogenic potential of the cells associated with the age-related changes observed in mouse skin, we isolated dFBs from skin at various ages and differentiated them into adipocytes in vitro. Whereas uncommitted E14 dFBs were only partially adipogenic, neonatal P1 dFBs were highly adipogenic, and this adipogenic potential gradually declined during postnatal development (from 3 weeks to 2 months of age) and was lost in 1-year-old dFBs (Figure 2F). Time-course analysis of differentiating neonatal dFBs showed that immature ADs with small lipid droplets were formed as early as post-differentiation day 2 (PD2), and by PD4~PD7, >90% of cells became mature ADs with large lipid droplets (Figure 2G). Gene expression analyses revealed four distinct expression kinetics: (1) Col1a1 and Thy1 mRNA expression was highest in undifferentiated cells and gradually decreased as cells converted to ADs; (2) Pdgfra, Sca1, Pref1, or Pparg1 mRNA expression was detected prior to differentiation, was further elevated on PD1~PD2, and then robustly decreased at PD4; (3) Camp expression was induced as early as PD1 and peaked around PD2; and (4) Pparg2, Adipoq, or Fabp4 mRNA expression was induced later, around PD2~PD4, and continued to increase as adipocytes matured (Figures 2H and 2l). Camp^{f/f}Pdgfra-cre dFBs or Camp^{f/f}Adipog-cre dFBs showed loss of Camp expression and secretion through differentiation in vitro (Figures S2E-S2G), confirming that these adipose precursor cells are the major cellular source of cathelicidin. The ability of differentiating neonatal dFBs to express Camp and Pparg2 mRNA (Figures 2J and S2H) and to secrete cathelicidin protein into conditioned medium (Figures S2I and S2J) was progressively lost in dFBs isolated from 3-week-old, 2-month-old, and 1-year-old skin. In contrast, adult dFBs produced higher Col1a1 mRNA expression during differentiation than neonatal dFBs (Figure 2J), suggesting that decreased adipogenic function is accompanied by increased fibrogenic function in adult dFBs. Functionally, the supernatant from differentiating P1 dFBs potently inhibited the growth of S. aureus (SA113 and USA300) (Figure 2K), whereas the age-related decline in antimicrobial protein expression correlated with decreased capacity of differentiating dFBs to inhibit the growth of S. aureus (Figures S2L and

Figure 2. Loss of Dermal Immature Fat and Adipogenic-Antimicrobial Function of Primary dFBs during Development and Aging of Mouse Skin

(A) Gomori Trichrome staining (top) or lipid BODIPY (green) and phalloidin (red) staining (bottom) of skin sections from mice at the indicated age (representative of n = 3–6 per group).

- (B) Hydroxyproline content (µg per mg of tissue) in mouse dorsal skin at the indicated age (representative of n = 3 per group).
- (C) Heatmap showing the mRNA expression kinetics of listed pAd or AD genes in mouse skin at the indicated age (average of n = 3 per group).
- (D) Camp mRNA expression kinetics in mouse skin at the indicated age (n = 3 per group).
- (E) Relative Camp mRNA expression in skin isolated from neonatal $Camp^{t/t}$, $Camp^{t/t}$ Pdgfra-cre, or $Camp^{t/t}$; Adipoq-cre neonatal littermates (n = 3 per group).
- (F) Phase-contrast images showing age-dependent alterations in the adipogenic potential of primary dFBs (representative of n = 3 per group).
- (G) Phase-contrast images showing time-course adipocyte differentiation from neonatal P1 dFBs (representative of n = 3 per group).
- (H) Heatmap showing kinetics of pAd or AD gene mRNA expression during adipocyte differentiation of P1 dFBs (average of n = 3 per group).
- (I) Bar graphs of mRNA expression kinetics of Camp or Col1a1 during adipocyte differentiation of P1 dFBs (average of n = 3 per group).
- (J) Camp or Col1a1 mRNA expression in undifferentiated dFBs or differentiated adipocytes (n = 3-5 per group).
- (K) Image of SA113 or USA300 growth on an agar plate or CFU count of bacterial growth in conditioned medium from P1 ADs or undifferentiated cells or DMEM (n = 3 per group).
- (L and M) Growth curve (L) or CFU count (M) of S. aureus in CM from undifferentiated dFBs or differentiated adipocytes at the indicated age (n = 3–5 per group). All error bars indicate mean \pm SEM. *p < 0.05, **p < 0.01, ***p < 0.001 (one-way ANOVA). Scale bars, 100 μ m. Please also see Figure S2.

S2M). Altogether, these data show a loss of immature dermal fat and that the adipogenic-antimicrobial function of dFBs occurs with age.

Activation of the TGF- β Pathway Is Associated with the Loss of Antimicrobial Function of dFBs

To better understand the change in the antimicrobial and adipogenic functions of dFBs, we profiled the transcriptomes of primary dFBs isolated at different ages by RNA sequencing (RNA-seq). Because fibroblast populations become heterogeneous during postnatal development (Driskell et al., 2013) (Figure S3A), we sorted Sca1⁺ dFBs from all postnatal groups to focus on the dFB population committed to the adipose lineage. Sca1 labeling purity was confirmed by flow cytometry (Figure S3B), and compared with Sca1⁺ dFBs, sorted Sca1⁻ dFBs were confirmed to be unable to differentiate into ADs (Figure S3C). Because dFBs lost their adipogenic function by 2 months of age (Figure 2E), we chose 2 months as the most advanced age group for RNA-seq analyses.

Principle-component analysis revealed a distinction in the transcriptomes of dFBs isolated from different age groups. E14 dFBs and 2-month-old Sca1+ dFB samples were clearly separated from P1 Sca1+ dFB samples (Figure 3A). Time-course analyses identified seven gene clusters with multiple Gene Ontologies (GOs) undergoing distinct temporal changes (Figures 3B and S3D-S3I). To identify top putative regulators that drive these age-associated changes, we performed Ingenuity Pathway Analysis (IPA) and identified TGF-β signaling as the top activated signaling pathway in 2-month-old Sca1+ dFBs compared with P1 Sca1+ dFBs (Figure 3C). IPA also predicted that TGF- β signaling activities were significantly different between dFBs from other age groups and P1 Sca1+ dFBs (Figures S3J and S3K). Consistently, RNA-seq and qRT-PCR analyses (Figures 3D-3G) revealed that the expression of the key genes in the TGFBR pathway, including Tgfbr1 or Tgfbr2, Tgfb1 or Tgfb2, and Inhba, was higher in 2-month-old than in P1 Sca1+ dFBs. The expression of several TGF-β pro-fibrotic genes downstream of TGF-β, including Acta2 (coding for alpha smooth muscle actin [SMA]), Ctgf, Spp1, Pai1, Mmp13, Saa3, and Il6, was strongly elevated in 2-month-old cells compared with P1 cells. In contrast, the expression of several pro-adipogenic genes, including Pref1, Pparg, Sca1, Lpl (Gregoire et al., 1998), and Dcn (a natural inhibitor of TGF-β signaling [Border et al., 1992]), was suppressed in 2-month-old cells compared with P1 cells. Similar to 2-month-old cells, E14 fibroblasts expressed and secreted significantly higher amounts of Tafb2 transcript and TGF-β2 protein than neonatal dFBs (Figures 3E and 3F). The expression of proadipogenic genes, including Pparg, Sca1, and Dcn, was suppressed in E14 compared with P1 cells, but profibrotic genes, including Acta2 and Spp1, were only moderately elevated in E14 cells, suggesting that the pro-fibrotic effect of TGF-β is preferentially suppressed in embryonic cells. Altogether, these results indicate that TGF-β could play a role in the age-related switch from pro-adipogenic to pro-fibrotic dFBs.

TGF- β 2 Drives Loss of Adipogenic-Antimicrobial Function in Neonatal dFBs

To determine whether the presence of TGF- β ligands is functionally relevant, we treated neonatal dFBs with recombinant mouse

TGF-β2. Doses as low as 0.1 ng/mL of TGF-β2 potently suppressed the adipogenic function of P1 cells, and at higher doses (3-10 ng/mL) it not only completely abolished adipogenic function but also triggered a fibrotic phenotype characterized by extensive cell striation and spindle-shaped morphology (Figure 4A). In parallel, the induction of adipocyte marker genes, secretion of cathelicidin and FABP4, and suppression of Col1a1 mRNA upon adipocyte differentiation were inhibited by TGF-β2 (Figures 4B and 4C). In undifferentiated P1 dFBs, TGFβ2 triggered a dose-dependent decrease in the expression of pro-adipogenic genes (Sca1, Pref1, Pparg1, and Dcn) and an increase in the expression of pro-fibrotic and inflammatory genes (Spp1, Acta2, Mmp13, Pai1, Ctgf, and II6) (Figures 4D and 4E). Similar results were also seen in neonatal dFBs treated with TGF-β1, except that TGF-β1 was three to ten times less potent than TGF-β2 (Figures S4A and S4B).

To characterize the dynamic interplay between pro-fibrotic and anti-adipogenic functions of TGF-β, we evaluated expression of Sca1 and SMA in PDGFRA+THY1+ dFBs by flow cytometry (Figure \$4C). Cultured neonatal PDGFRA+THY1+ dFBs exhibited high Sca1 and low SMA mRNA expression. Treatment with TGFβ2 or TGF-β1 for 2 days led to a rapid dose-dependent decrease in Sca1 and increase in SMA expression (Figures 4F, 4G, and S4D). Flow-cytometry analyses of cultured dFBs from various ages revealed that, whereas neonatal PDGFRA+THY1+ dFBs were mostly Sca1^{hi}SMA^{lo}, dFBs gradually lost Sca1 and gained SMA expression with age, and by 1 year of age, most cells were Sca1loSMAhi (Figures 4H and 4I). Cultured 2-month-old and 1-year-old dFBs strongly resembled neonatal dFBs treated for 2 days with TGFβ2 (Figure 4F). The antimicrobial activity of differentiating neonatal dFBs against S. aureus was completely suppressed after the addition of TGF-β2 (Figures 4J, 4K, and S4E). These results demonstrate that TGF-β2 is a potent suppressor of dFBs' capacity to differentiate into ADs and provide antimicrobial activity.

TGF- β Exerts Anti-adipogenic Effects on dFBs by Activating the TGFBR-SMAD2/3 Pathway

To understand the signaling pathway mediating the effect of TGF- β on dFBs, we evaluated downstream signaling molecules of the TGF-β pathway. Phosphoblotting analyses of neonatal dFBs treated with TGF-β2 showed that TGF-β2 induced a transient increase in SMAD2/3 and AKT phosphorylation (Figure 5A). To determine the role of SMAD3 and AKT in the effects of TGF- β , we applied small pharmacological inhibitors specific to SMAD3 (SIS3) (Jinnin et al., 2006), AKT (Wortmannin) (Zhang et al., 2016), or TGFBR SB431542 (SB) (Inman et al., 2002; Mordasky Markell et al., 2010). Pretreatment with either SMAD3 or TGFBR inhibitors, but not an AKT inhibitor, rescued TGF-β-driven suppression of Pparg1 and induction of Ctgf mRNA expression (Figure 5B) and restored the adipogenic function and the ability of neonatal dFBs to produce and secrete cathelicidin (Figures 5C-5D and S5A). These results demonstrate that TGF-β exerts its pro-fibrotic and anti-adipogenic effects on dFBs via the TGFBR-SMAD2/3 pathway.

Inhibition of TGFBR Function Boosts dFB Adipogenic Potential and Enhances Resistance to Skin Infection

To test the hypothesis that TGF- β 2 is responsible for the agedependent loss of adipogenic capacity of dFBs, we treated

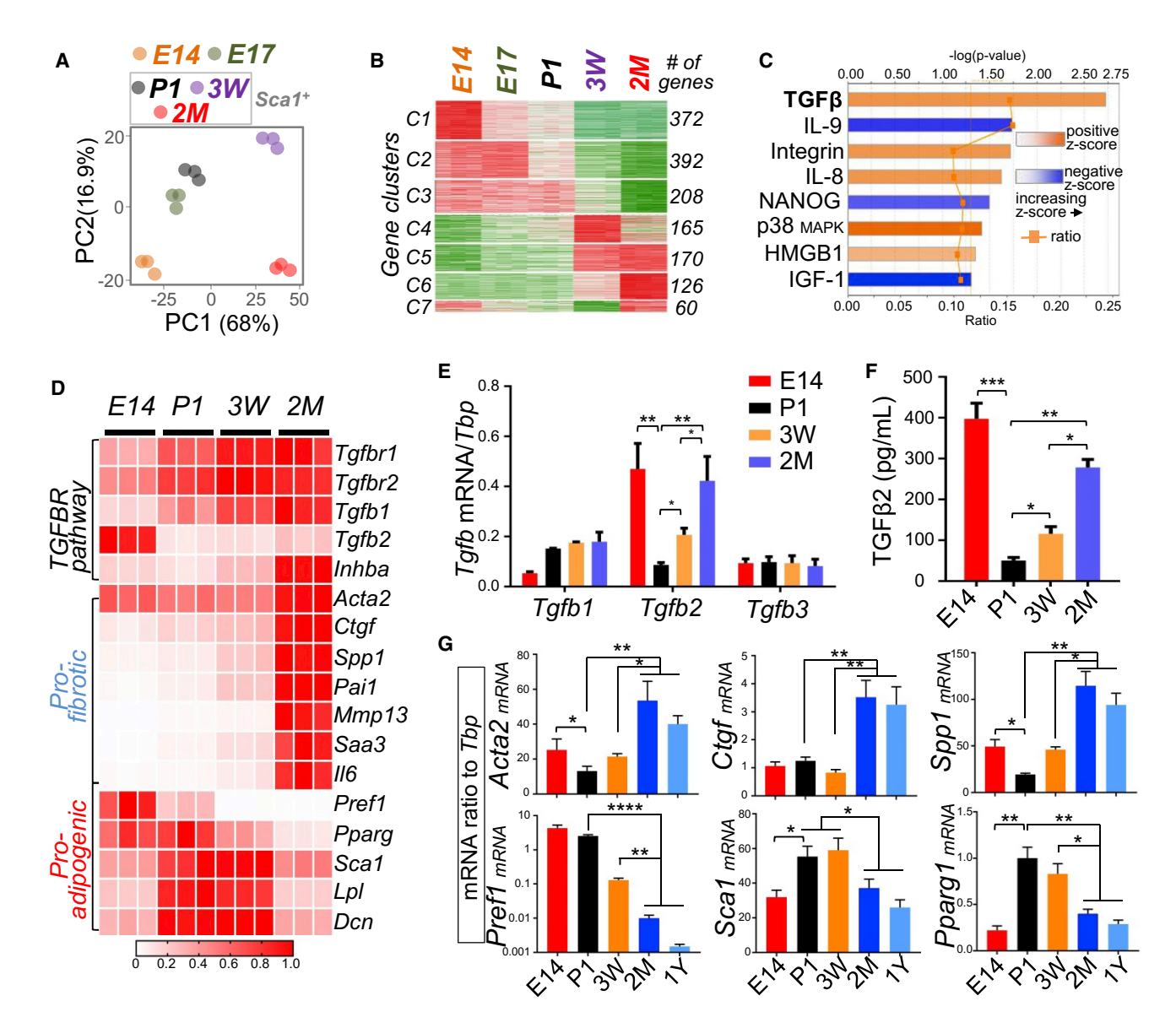


Figure 3. Activation of the TGF-β Pathway Is Associated with the Loss of Antimicrobial Function of dFBs

(A) Principle-component-analysis plot for RNA-seq shows differential clustering of E14, E17, or Sca1⁺ cells sorted into P1, 3-week-old, and 2-month-old dFBs. Dots with the same color represent biological replicates in the indicated age group (n = 3 per age group).

(B) Time-course analyses by maSigPro identified seven gene clusters with distinct expression dynamics in dFBs from E14 to 2 months as indicated. The number of genes in each cluster is indicated on the right.

(C) Ingenuity Pathway Analysis identified several signaling pathways that were activated (orange) or inhibited (blue) in 2-month-old Sca1⁺ dFBs compared with P1 Sca1⁺ dFBs. Respective -log(p values), Z scores, and ratios are shown for each pathway. The calculated Z score indicates a pathway with genes exhibiting overall increased mRNA (orange bars) or decreased mRNA (blue bars) expression. The ratio (orange dots connected by a line) indicates the ratio of dataset genes that map to the pathway to the total number of genes that map to the same pathway, e.g., >15% for TGF-β signaling.

(D) Heatmap showing relative mRNA expression (based on RNA-seq-derived RPKM [reads per kilobase of transcript per million mapped reads] values) of a panel of TGFBR pathway genes, pro-fibrotic genes, or pro-adipogenic genes in primary dFBs (average of n = 3 per group).

(E) qRT-PCR analyses showing mRNA expression of TGF-β-family genes (ratio to Tbp) in dFBs at the indicated ages (n = 3 per group).

(F) TGF-β2 secretion (pg/mL) in the conditioned medium of dFBs was quantified by ELISA (n = 3 per group).

(G) qRT-PCR analyses validating age-dependent changes in mRNA expression of pro-adipogenic genes (Pref1, Sca1, and Pparg1) or pro-fibrotic genes (Acta2, Ctgf, and Spp1) (n = 3 per group).

All error bars indicate mean ± SEM. *p < 0.05, **p < 0.01, ***p < 0.001 (one-way ANOVA). Please also see Figure S3.

primary dFBs isolated from mice of various ages with SB in culture for 3 days. Inhibition of TGFBR reversed the loss of Sca1 and gain of SMA observed in PDGFRA+THY1+ dFBs during aging (Figures 5E-5G). The age-associated suppression of pro-adipogenic Pparg1 and increased expression of the pro-fibrotic Spp1 were also reversed by SB treatment (Figures 5H and 5I).

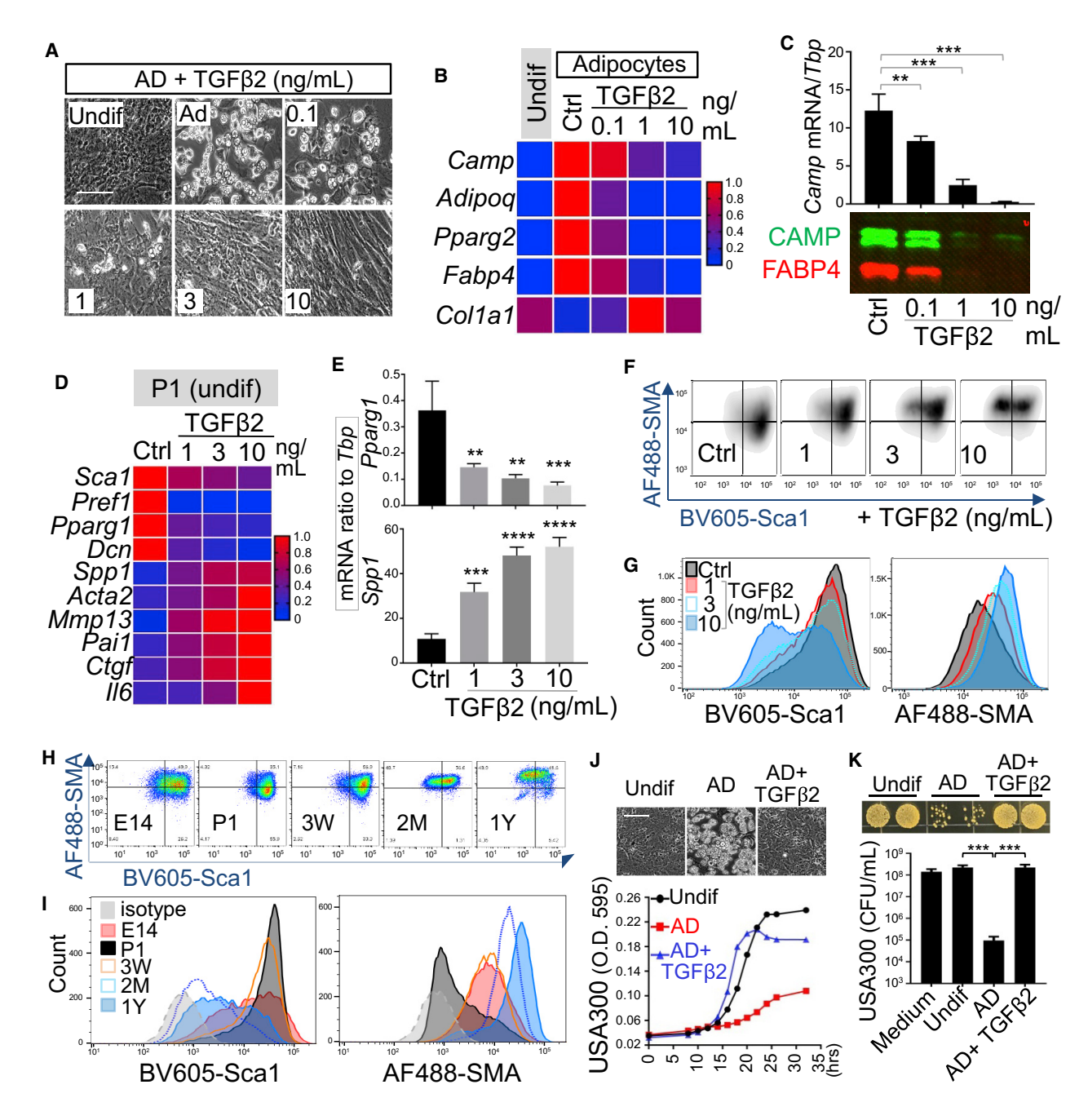


Figure 4. TGF-β2 Drives a Loss of Adipogenic-Antimicrobial Function of Neonatal dFBs

(A-C) Neonatal dFBs were treated with increasing doses of TGF- $\beta 2$ and differentiated into adipocytes. (A) Phase-contrast images showing adipocyte formation at day 4 (representative of n = 3 per group). Scale bars, 100 μ m. (B) Heatmap showing the effect of TGF- $\beta 2$ in suppressing the mRNA expression of adipocyte genes (average of n = 3 per group). (C) Camp mRNA expression was measured by qRT-PCR (top bar graphs) and CAMP and FABP4 secretion (lower western blots) (representative of n = 3 per group).

(D-G) Neonatal P1 dFBs were treated with increasing doses of TGF- β 2 for 2 days under undifferentiated conditioned. Heatmap (D) or bar graphs (E) show relative expression of pro-adipogenic or pro-fibrotic genes as indicated (n = 3 per group). Also shown are flow-cytometry plots (F) or overlaid histograms (G) of Sca1 and SMA (representative of n = 3 per group).

- (H) Flow-cytometry plots of Sca1 and SMA in cultured PDGFRA $^+$ THY1 $^+$ dFBs at the indicated age.
- (I) Overlaid histogram of the Sca1 or SMA expression shown in (H) (representative of n = 3 per group).
- (J) Growth curve of USA300 in CM from undifferentiated dFBs or differentiated adipocytes (n = 3–5 per group). Inset phase-contrast images show the effect of TGF-β2 in suppressing adipocyte formation. Scale bars, 100 μm.

(K) Bacterial growth image on agar plate or CFU count of USA300 growth at 20 hr in CM from adipocytes treated with or without TGF-β2 as indicated (n = 3–5 per group).

All error bars indicate mean \pm SEM. *p < 0.05, **p < 0.01, ***p < 0.001 (one-way ANOVA). Please also see Figure S4.

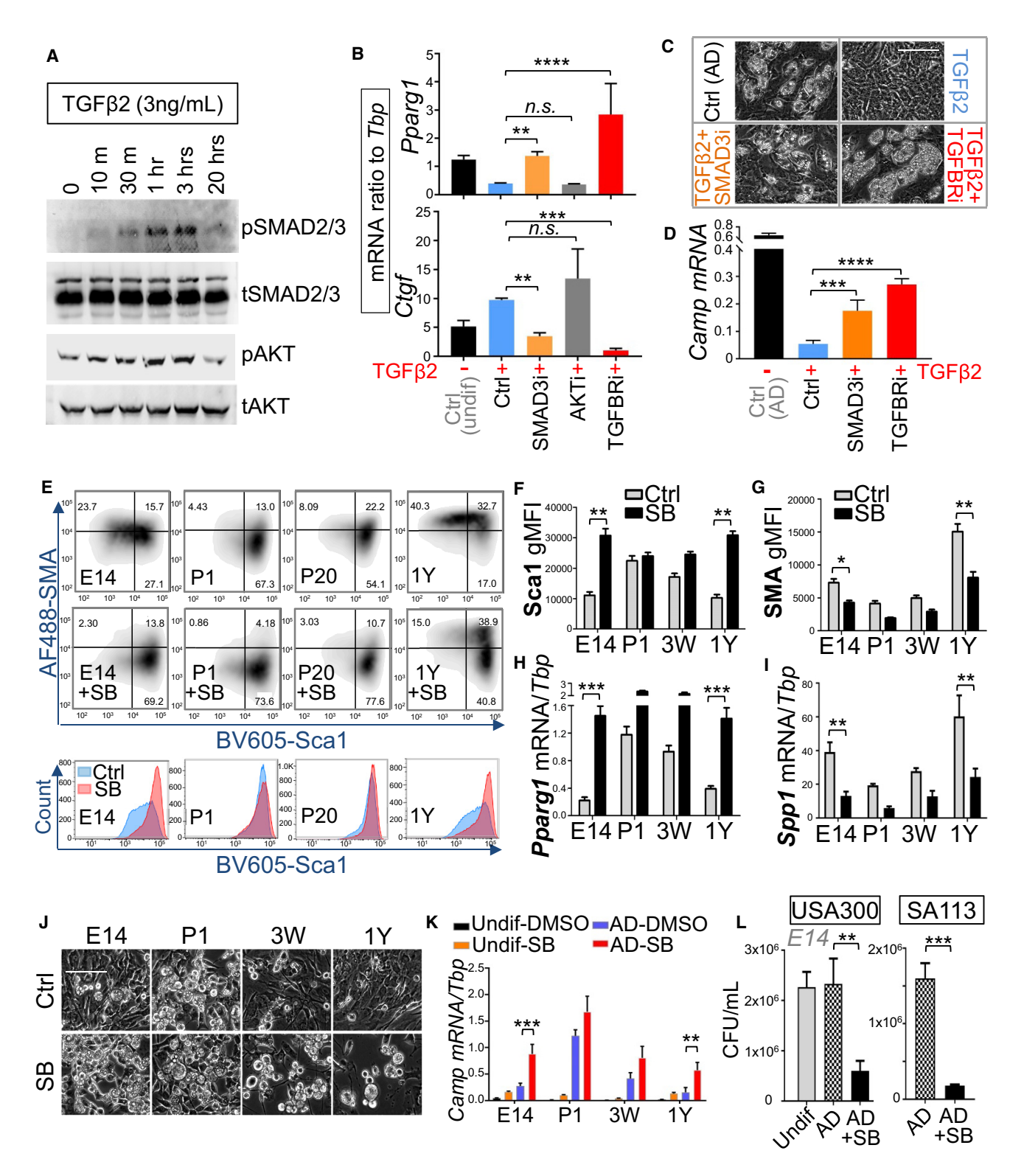


Figure 5. TGF-β Mediates Its Pro-fibrotic and Anti-adipogenic Function by Activating the TGFBR-SMAD2/3 Pathway in dFBs
(A) Western blot analyses of phosphor or total SMAD2/3 or AKT in P1 dFBs treated with 3 ng/mL TGF-β2 for the indicated time.
(B) qRT-PCR analyses of *Pparg1* or *Ctgf* mRNA expression in neonatal dFBs pre-treated with specific inhibitors for SMAD3 (SIS3, 2 μM), PI3K-AKT (0.5 μM Wortmannin), or TGFBR (SB431542, SB, 5 μM) and then TGF-β2 for 24 hr (n = 3 per group).
(C and D) TGF-β2-mediated loss of adipogenic function of neonatal dFBs can be rescued by SMAD3 or TGFBR inhibitor, as shown by phase-contrast images (C) or qRT-PCR analysis of *Camp* mRNA expression (D) (n = 3 per group). Scale bars, 100 μm.

Inhibition of TGFBR enabled embryonic and adult dFBs to differentiate into mature adipocytes (Figure 5J) and express cathelicidin (Figure 5K). *Col1a1* expression was also suppressed upon TGFBR inhibition (Figure S5B). Furthermore, the antimicrobial potential of the conditioned medium from differentiating embryonic dFBs was enhanced when TGFBR was inhibited (Figure 5L).

TGF- β Signaling Is Active in the Dermis and Promotes Loss of Antimicrobial Defense in Mice

To investigate the role of the TGF-β pathway in dFBs in vivo, we examined activation of phosph-SMAD2/3 (pSMAD2/3) and the abundance of TGF-β in mice of various ages. Increased pSMAD2/3 was seen in adult dermis (3 weeks to 2 years of age) compared with neonatal dermis (Figure 6A). P1 and 3-week-old skin showed random pSMAD2/3 distribution throughout the dermis, whereas 2-month- to 2-year-old skin showed prominent pSMAD2/3 staining in the dWAT layer (Figure 6A). This suggests that pSMAD2/3 signals might be preferentially turned on only in the committed pAds in dWAT during adulthood. Circulating TGF-β2 concentrations in serum were high in neonatal (P1-P7) and young adult mice (3 weeks of age) but then declined progressively with advancing age (2 months to 2 years of age) (Figure 6B). In contrast, circulating TGF-β1 concentrations were low in neonates and became elevated from adulthood through aging (Figure 6C). To determine whether TGF-β might promote dermal fat loss in adulthood, we treated adult mice intradermally with SB for 5 days (Figure 6D). SB-treated skin showed notable expansion of the dWAT layer (Figure 6D) and higher expression of Camp and Adipoq and lower expression of pro-fibrotic genes (Col1a1 and Ctaf) than non-SB-treated skin (Figure 6E).

To determine whether these observations could translate into reduced susceptibility to infection in vivo, we administrated SB after infecting 1-year-old adult mouse skin with S. aureus strain USA300 (Figure 6F). Treating the infected mice with SB improved resistance to S. aureus skin infection, as shown by a decrease in lesion size and bacterial CFU at the infection edge and in the central area of the lesion (Figures 6F and 6G). qRT-PCR analyses revealed that SB administration not only increased the expression of pAd- or AD-related genes, including Pdgfra and Camp, but also suppressed expression of the pro-fibrotic gene Spp1 at the infection site (Figures 6H and S5C). The reactive adipogenesis responses, including enhanced adipocyte hyperplasia and cathelicidin protein production, upon infection were enhanced in SB-treated mice compared with control mice (Figure 6I). In addition, to inhibit TGFBR specifically in dFBs, we generated conditional heterozygous deletion of Tgfbr2 by crossing Tgfbr2flox/flox mice to Pdgfra-cre (Tgfbr2flox/+Pdgfra-cre) mice (Figure 6J). No homozygous Tgfbr2flox/Pdgfra-cre offspring were generated despite extensive breeding, and thus experiments were conducted only with heterozygous offspring. dFBs

isolated from Tgfbr2^{flox/+}Pdgfra-cre mice expressed ~50% less Tgfbr2 mRNA than WT dFBs (Figure S5D). Tgfbr2flox/+ Pdgfra-cre dFBs were less responsive to exogenous TGF-β2 treatment, as shown by an impaired induction of profibrotic genes, including Ctgf, Acta2, and Spp1 (Figures 6K and 6L). Importantly, when mice were subjected to S. aureus infection, the fibrotic response in the infected skin was significantly reduced in comparison with that of WT controls (Figure 6M). Furthermore, more lipid droplets and cathelicidin protein were detected in the infected Tgfbr2^{flox/+}Pdgfra-cre dermis than in infected WT controls (Figure 6N). Overall bacterial abundance was lower, but not statistically significant, in the infected skin of Tgfbr2^{flox/+}Pdgfra-cre mice than in WT controls (Figures S5E-S5G), suggesting that heterozygous deletion of *Tgfbr2* in Pdgfra⁺ dFBs might not be sufficient to drive a clinical phenotype. These changes demonstrate that TGF-B critically drives age-dependent loss of the innate antimicrobial function of the skin.

TGF-β Promotes Loss of Adipogenic and Antimicrobial Defense Function of Primary Human Dermal Fibroblasts

To determine whether our observations in mice might also be relevant to humans, we evaluated dWAT in human skin samples (Caucasian; non-obese) from neonates (gestational weeks [GW] 29-38), young adults (18-25 years of age), mid-age adults (50-65 years of age), and elderly donors (>75 years of age). Neonatal skin, either preterm (GW 29-32) or full term (GW 38-40), contained a large volume of dWAT and a thin dermis, whereas in adulthood dWAT volume became gradually reduced and was eventually lost in mid-age and elderly skin samples (Figures 7A and S6A). A similar trend of dWAT loss during adulthood was also observed in human skin biopsies (Chinese; non-obese) collected from young children (2-6 years of age), young adults (18-25 years of age), and mid-age adults (50-65 years of age) (Figure S6B). Similar to that in mouse skin, the mRNA expression of PREF1 or human CAMP was significantly higher in human neonatal skin than in mid-age or elderly skin samples (Figures 7B and S6C), Immunostaining of human skin sections for the human cathelicidin peptide LL-37 showed that it was abundantly expressed in neonatal dermal ADs but not in the larger ADs in aged skin (Figure S6D). dWAT loss in adulthood coincided with an increase in dermal thickness, fibrogenesis (as measured by collagen staining), and COL1A1 mRNA upregulation (Figures 7A, S6A, and S6E). In elderly human skin, similar to 2-year-old mouse skin, a decrease in dermal thickness, collagen content, and COL1A1 mRNA expression was observed (Figures 7A, S6A, and S6E), suggesting that prolonged activation of dFBs might eventually lead to loss of cells' pro-fibrogenic function in elderly skin.

To determine whether TGF- β can inhibit adipogenic function of human neonatal dFBs, we differentiated primary neonatal dFBs isolated from five donors into adipocytes with or without TGFBR

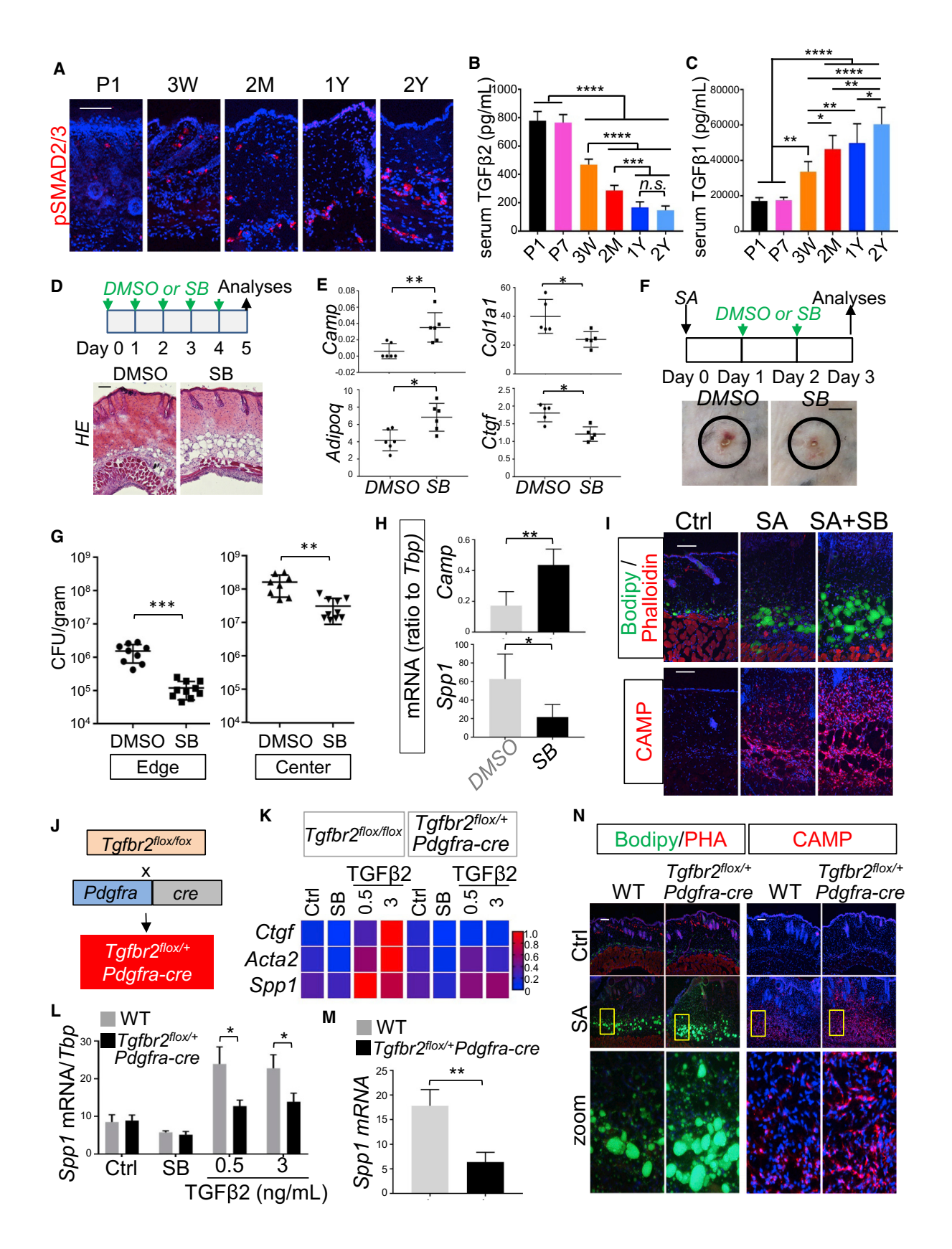
⁽E) Flow-cytometry plots of Sca1 and SMA (top) or overlaid histogram of Sca1 (bottom) in PDGFRA+THY1+ dFBs treated with TGFBR inhibitor SB431542 (representative of n = 3 per group).

⁽F and G) Quantification of the gMFI of the Sca1 or SMA expression shown in (E) (n = 3 per group).

⁽H and I) Pparg1 or Spp1 mRNA expression in dFBs treated with SB or DMSO control for 2 days (n = 3 per group).

⁽J) Phase-contrast images of dFBs differentiated into adipocytes in the presence of SB or DMSO control (representative of n = 3 per group). Scale bars, 100 μm. (K) Camp mRNA expression in undifferentiated or adipocyte-differentiated dFBs treated with SB or DMSO control (n = 3 per group).

⁽L) Inhibition of TGFBR by SB restored the antimicrobial activity of E14 dFBs, as shown by CFU counts of USA300 or SA113 growth at 20 hr (n = 3–5 per group). All error bars indicate mean \pm SEM. *p < 0.05, **p < 0.01, ***p < 0.001 (one-way ANOVA). Please also see Figure S5.



inhibitor or recombinant TGF-β2. Neonatal dFBs from three donors had high adipogenic capacity and highly expressed CAMP and FABP4 mRNA, both of which could be completely inhibited with TGF-β2 treatment (Figures S7A and 7C). In contrast, dFBs isolated from the other two neonatal donors had low basal adipogenic capacity but became highly adipogenic and expressed high CAMP and FABP4 mRNA when TGFBR inhibitor (SB) was added (Figure S7A and Figure 7C). Adipogenic capacity positively correlated with PPARG mRNA expression in undifferentiated cells before or after SB treatment (Figure 7D).

To define the role of TGF- β in controlling the pro-adipogenic and pro-fibrotic functions of human dFBs, we next focused on the neonatal dFBs with low basal adipogenic capacity. Under basal conditions, these cells had a notable fibrotic morphology, characterized by stratification and clustering of cells into aggregates (Figure 7E), and this phenotype was further exacerbated upon treatment with TGF-β2, but was potently diminished upon treatment with SB (Figure 7E). Flow-cytometry analysis for SMA expression revealed that untreated cells were composed of mixed populations with low, medium, and high expression of SMA, and TGFBR inhibitor treatment shifted these cell populations to mostly an SMAlo state, whereas TGF-β2 treatment shifted them toward mostly an SMAhi state (Figure 7F). These cells expressed low basal PPARG mRNA and high ACTA2 and CTGF (fibrotic gene) mRNA, and recombinant TGF-β2 further decreased PPARG and increased ACTA2 and CTGF expression, whereas SB treatment strongly increased PPARG and almost completely suppressed CTGF expression (Figures S7B and S7C). Thus, by default, these cells were weakly adipogenic, and treatment with TGFBR inhibitor restored their adipogenic function and ability to express CAMP (Figures 7E and S7C). These results demonstrate that the endogenous TGF-β pathway is constitutively active in neonatal human dFBs with low basal adipogenic capacity and drives them to shift from a pro-adipogenic to a pro-fibrotic phenotype. Furthermore, antimicrobial assavs using conditioned medium collected from undifferentiated and differentiated human neonatal dFBs treated with SB demonstrated that only differentiating adipocytes treated with TGFBR inhibitor significantly suppressed growth of two S. aureus strains, SA113 and USA300 (Figure 7G). In addition, inhibition of TGFBR in primary adult dFBs isolated from four mid-age adult donors showed a significant decrease in mRNA expression of CTGF and COL1A1 and an increase in PPARG expression (Figure 7H), suggesting that the TGF-β-mediated switch from proadipogenic to pro-fibrotic also occurs in human adult cells. Together, these results are consistent with observations in mice and demonstrate that TGF-β drives loss of the adipogenic-antimicrobial function of primary human dFBs.

DISCUSSION

Effective defense against S. aureus infections relies on a proper immune response from skin-resident cells, including adipogenic dFBs (Zhang et al., 2015) and lymphoid and myeloid immune cells, such as T lymphocytes, neutrophils, and macrophages (Dillen et al., 2018; Feuerstein et al., 2015; Miller et al., 2006). It is well established that myeloid-derived innate and adaptive immunity is deficient early in life (Futata et al., 2012; Georgountzou and Papadopoulos, 2017; Shaw et al., 2013), suggesting that the non-myeloid-resident cells, such as adipogenic dFBs, could provide critical host defense against invasive S. aureus infections, especially in early life. However, age-related changes in the innate immune function of adipogenic dFBs have been unexplored.

We have shown that PDGFRA+THY1hi dFBs responded to infection by producing cathelicidin through reactive adipogenesis, and loss of this antimicrobial response led to increased susceptibility to S. aureus infection. We have also shown that neonatal skin immunity was composed of highly adipogenic PDGFRA+THY1hi dFBs and a large volume of immature dermal fat that highly expressed cathelicidin. These results suggest that adipogenic dFBs and immature fat layers could function as critical antimicrobial protective components in neonatal skin immunity, when myeloid and lymphoid immune systems are not yet mature. During postnatal development and in adulthood, the PDGFRA+THY1hi dFB population, immature fat, and the adipogenic potential of dFBs became progressively lost as the myeloid immune system matured, suggesting that the latter compensates for the loss of innate immune function of adipogenic dFBs.

To identify the underlying mechanisms for age-dependent changes in adipogenic function of dFBs, we cultured primary dFBs isolated from mouse skin at different ages and observed a drastic pro-adipogenic-to-pro-fibrotic switch that was age

Figure 6. Inhibition of TGFBR Function Boosts dFBs Adipogenic Potential and Enhances Resistance to Skin Infection

(A) pSMAD2/3 immunostaining of skin sections from mice at the indicated age (representative of n = 3 per group).

(B and C) Measurement of serum concentrations of TGF-β2 (B) or TGF-β1 (C) in mice at the indicated age (n = 3-6 per age group).

(D and E) C57BL6 WT mice (2 months old, male) were treated i.d. with DMSO (control) or SB daily for 5 days, and skin samples were collected for H&E (D) or qRT-PCR (E) analyses as indicated (representative of n = 5-6 per group).

(F) Representative skin-lesion pictures of 1-year-old C57BL6 mice infected with S. aureus and then treated i.d. with DMSO or SB (n = 5 per group).

(G) Bacterial CFU count was measured from the infection edge or center area at day 3 (n = 5 per group).

(H) Camp and Spp1 mRNA expression in S. aureus-infected skin (n = 3-5 per group).

(I) Representative BODIPY staining or cathelicidin (CAMP) staining in infected skin (n = 3-5 per group). Nuclei were stained with DAPI (blue).

 $(J) \ Conditional \ heterozygous \ \textit{Tgfbr2}^{flox/flox} \ mice \ with \ \textit{Pdgfra-cre}, \ was \ achieved \ through \ the \ breeding \ of \ \textit{Tgfbr2}^{flox/flox} \ mice \ with \ \textit{Pdgfra-cre}, \ was \ achieved \ through \ the \ breeding \ of \ \textit{Tgfbr2}^{flox/flox} \ mice \ with \ \textit{Pdgfra-cre}, \ was \ achieved \ through \ the \ breeding \ of \ \textit{Tgfbr2}^{flox/flox} \ mice \ with \ \textit{Pdgfra-cre}, \ was \ achieved \ through \ the \ breeding \ of \ \textit{Tgfbr2}^{flox/flox} \ mice \ with \ \textit{Pdgfra-cre}, \ was \ achieved \ through \ the \ breeding \ of \ \textit{Tgfbr2}^{flox/flox} \ mice \ with \ \textit{Pdgfra-cre}, \ was \ achieved \ through \ the \ breeding \ of \ \textit{Tgfbr2}^{flox/flox} \ mice \ with \ \textit{Pdgfra-cre}, \ was \ achieved \ through \ the \ breeding \ of \ \textit{Tgfbr2}^{flox/flox} \ mice \ with \ \textit{Pdgfra-cre}, \ was \ achieved \ through \ the \ breeding \ of \ \textit{Tgfbr2}^{flox/flox} \ mice \ with \ \textit{Pdgfra-cre}, \ was \ achieved \ through \ the \ breeding \ of \ \textit{Tgfbr2}^{flox/flox} \ mice \ with \ \textit{Pdgfra-cre}, \ was \ achieved \ through \ the \ \textit{Tgfbr2}^{flox/flox} \ mice \ with \ \textit{Pdgfra-cre}, \ was \ achieved \ through \ thr$

(K and L) Primary mouse dFBs (WT or Tgfbr2 flox/+Pdgfra-cre) were treated with increasing doses of TGF-β2, and induction of Ctgf, Acta2, and Spp1 is shown in a heatmap (K) or bar graph for Spp1 (L) (n = 3 per group).

(M and N) WT or Tgfbr2 flox/+Pdgfra-cre mice were infected i.d. with S. aureus. (M) mRNA expression of profibrotic gene Spp1 in infected skin (ratio to Tbp) (n = 3-5 per group). (N) Skin biopsies were subjected to BODIPY staining or cathelicidin staining as indicated (representative of n = 3-5 per group). Nuclei were stained with DAPI (blue).

All error bars indicate mean ± SEM. *p < 0.05, **p < 0.01, ***p < 0.001 (one-way ANOVA). Scale bars, 100 μm. Please also see Figure S1.

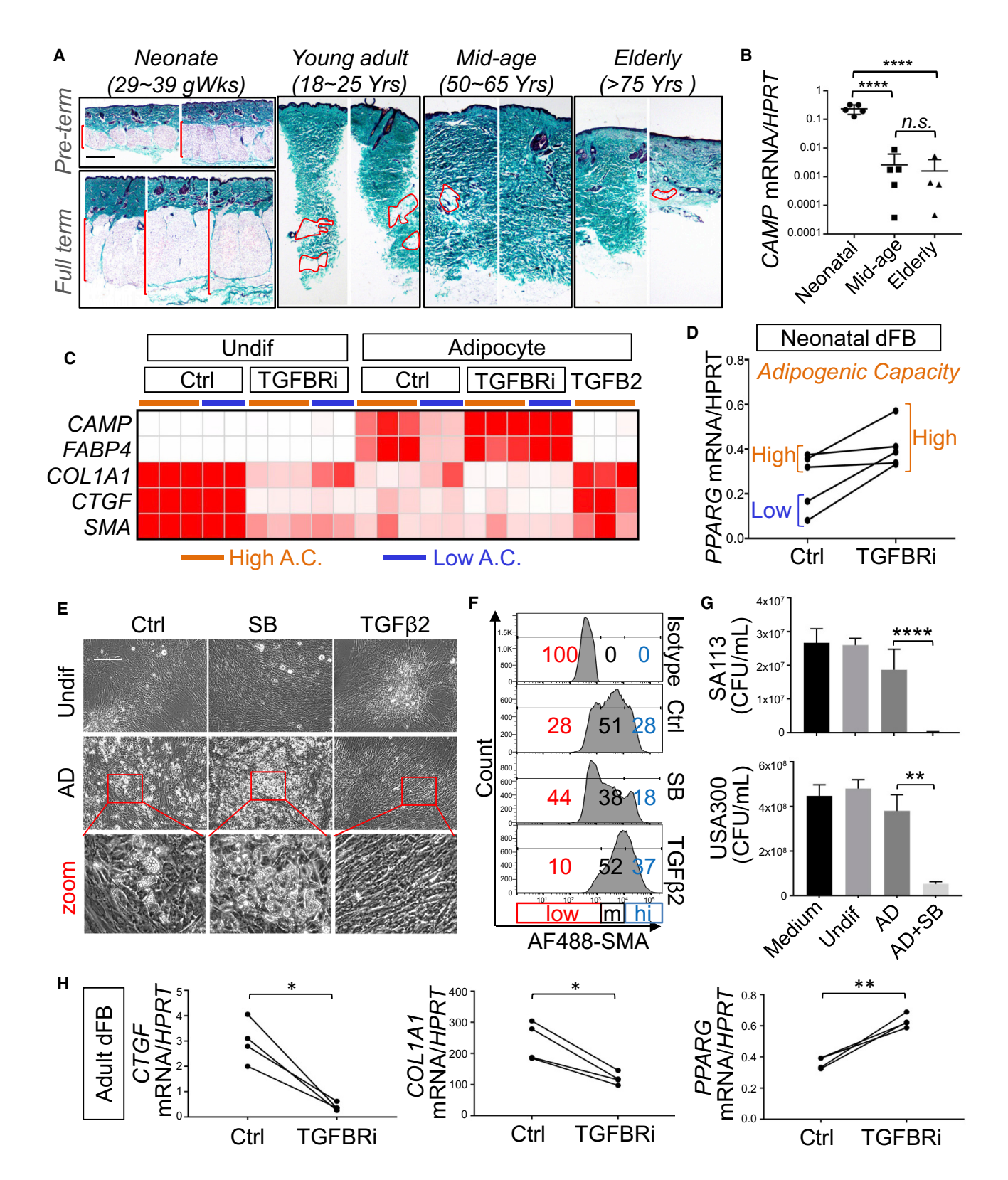


Figure 7. TGF- β Promotes Loss of Adipogenic and Antimicrobial Defense Function of Primary Human Dermal Fibroblasts

(A) Representative collagen-trichrome-staining images of human back skin sections from neonates (pre-term, gestation weeks [GW] 29–32; full-term, GW 38–40), young adults (18–25 years of age), mid-age adults (50–65 years of age), and elderly adults (>75 years of age). All subjects were white Caucasians (n = 3–6 per age group). dWAT is highlighted by red lines. Scale bars, 100 μm.

dependent: neonatal dFBs were highly adipogenic and potently inhibited bacterial growth, whereas adult cells gained profibrotic features, and both embryonic and adult dFBs had low adipogenic capacities and were not able to control bacterial growth. On the basis of RNA-seq analysis, we hypothesized a key role for TGF- β and confirmed it by reproducing the phenotype of adult or aged cells after treatment of neonatal dFBs with recombinant TGF-β2 and by rescuing loss of function in embryonic, adult, or aged dFBs after administration of a pharmacological inhibitor of TGFBR or via targeted genetic deletion. Administration of TGF-β inhibitor or targeted heterozygous deletion of Tgfbr2 in Pdgfra+ dFBs was also effective in vivo at restoring the reactive adipogenesis-antimicrobial defense function of dFBs in adult mice. Although the pro-fibrotic (Lakos et al., 2004) and anti-adipogenic (Choy and Derynck, 2003) functions of TGF-β pathways are already known, our results identify these fundamental functions of TGF-β as a key regulatory mechanism controlling the innate antimicrobial function of dFBs.

In vitro, Tgfb2 was the most abundant TGF-β isoform expressed by dFBs, and its expression correlated with the agerelated loss of adipogenic potential. TGF-β2 was found to be three to ten times more potent than TGF-β1 in triggering the adipogenic-to-pro-fibrotic switch in neonatal dFBs. In vivo, circulating TGF-β2 concentrations in mouse serum were high early in life (from P1 to P3 weeks) and then declined from adulthood through aging, whereas circulating TGF-β1 concentrations were low in neonates and became elevated with advancing age. We posit that a high serum concentration of TGF-β2 early in life might drive the rapid loss of adipogenic function of neonatal dFBs during postnatal development, whereas a decline in TGF-β2 serum concentration later in life might be compensated by rising TGF-β1. TGF-β2 can also be produced by other skin cell types, such as hair follicle keratinocytes and dermal papilla cells (Hibino and Nishiyama, 2004; Soma et al., 2002), and TGF-β2 could synergize with TGF-β1, which is abundantly produced by immune cells, such as macrophages (Keophiphath et al., 2009) and regulatory T cells (Bommireddy and Doetschman, 2007). Alternatively, endogenous production of TGF-β from adipocytes or surrounding stromal cells could provide a source for autocrine or paracrine suppression of adipocyte progenitors. Future studies will be needed to determine the cellular source of these TGF-β ligands.

Dermal fibroblasts are the major mesenchymal cell type in the skin, and these cells exhibit considerable functional diversity, which was also observed in our culture system. Primary mouse neonatal dFB cultures appeared highly homogeneous (>90% of cells were Sca1^{hi}SMA^{lo}), whereas adult dFBs appeared heterogeneous with mixed populations of Sca1^{hi-lo} and SMA^{lo-hi}

cells in culture. The Sca1loSMAhi dFBs harbored a myofibroblast-like gene signature (Hinz et al., 2012; Lee et al., 2010) and exhibited higher mRNA expression of pro-fibrotic genes (such as Acta2, Ctgf, and Spp1) and lower expression of pro-adipogenic expression (such as Pref1 and Pparg1) than Sca1hiSMAlo neonatal dFBs. This adipogenic-to-pro-fibrotic switch by adult cells could be reversed upon inhibition of TGFBR, suggesting that the plasticity between distinct phenotypic subpopulations of dFBs might be controlled by TGF-β. Analogous two-way conversion between myofibroblasts and adipogenic fibroblasts has been reported in several recent studies using genetic lineage-tracing tools in mice. In the mouse model of idiopathic pulmonary fibrosis, lung lipogenic fibroblasts have been observed to differentiate into myofibroblasts during early fibrosis formation, and later, during resolution of fibrosis, the population of newly formed myofibroblasts switches back to lipogenic fibroblasts (El Agha et al., 2017). In the skin, myofibroblasts that accumulate in the bleomycin-induced mouse model of scleroderma originate from Adipoq-positive intradermal progenitors (Marangoni et al., 2015). Furthermore, myofibroblasts formed during early skin wound healing give rise to new adipocytes that regenerate de novo during later stages of wound healing around de novo hair follicles (Plikus et al., 2017). Highly relevant to our work, these studies suggest that the pool of adipogenic fibroblasts in the skin or lung can switch between a profibrotic phenotype (such as myofibroblasts) during injury and a pro-adipogenic phenotype during injury resolution. Our results here suggest that TGF- β might be the key factor that regulates this plasticity between distinct phenotypic subpopulations of dFBs. Future studies are needed to identify the endogenous TGFBR inhibitor that converts pro-fibrotic dFBs to the adipogenic lineage.

In conclusion, these observations have uncovered that an age-dependent activation of the TGF- β pathway attenuates adipogenic function of dermal fibroblasts and promotes a subsequent loss of antimicrobial defense by dermal fat. This work provides insights into how activation of TGF- β negatively affects skin defense against infection and suggests that small molecules that suppress TGFBR might be an effective therapeutic to combat skin infections.

STAR*METHODS

Detailed methods are provided in the online version of this paper and include the following:

- KEY RESOURCES TABLE
- CONTACT FOR REAGENT AND RESOURCE SHARING

(B) qRT-PCR analyses of *CAMP* mRNA expression (ratio to housekeeping *HPRT*) in human neonatal, mid-age, or elderly skin as indicated (n = 4–5 per group). (C) Human dFBs isolated from five neonatal donors were differentiated to adipocytes with or without TGFBR inhibitor or TGF- β 2. The heatmap shows the mRNA expression of the indicated genes in undifferentiated or differentiated cells with high (orange line, n = 3) or low (blue line, n = 2) basal adipogenic capacity (AC). (D) qRT-PCR analysis of *PPARG* mRNA expression in neonatal dFBs (with high or low basal AC) treated with or without TGFBR inhibitor for 48 hr (n = 5 per group). (E–G) Primary human neonatal dFBs (with low basal AC) were differentiated into adipocytes with or without TGFBR inhibitor (SB) or recombinant TGF- β 2. (E) Phase-contrast images (representative of n = 3 per group). Scale bars, 200 μ m. (F) Flow-cytometry histogram of SMA expression in undifferentiated dFBs treated with SB or TGF- β 2 (representative of n = 3 per group). (G) CFU count of *S. aureus* USA300 growth at 20 hr in CM from undifferentiated cells or adipocyte differentiated cells as indicated (n = 3–5 per group).

(H) Primary adult human dFBs were isolated from four mid-age donors' back skin. Also shown is qRT-PCR analyses of CTGF, COL1A1, and PPARG1 in adult dFBs treated with vehicle control or TGFBR inhibitor (n = 3 or 4 per group).

All error bars indicate mean ± SEM *p < 0.05, **p < 0.01, ***p < 0.001 (one-way ANOVA). Please see also Figure S6 and S7.

• EXPERIMENTAL MODEL AND SUBJECT DETAILS

- O Animals and animal care
- O Mouse model of S. aureus skin infection

METHOD DETAILS

- O Chemicals, antibodies and dyes
- O Human skin sample collection
- Histology, collagen trichrome staining and immunohistochemistry (IHC)
- O Primary dermal fibroblast isolation and culture
- Flow cytometry and analysis (FACS)
- Reverse transcription-quantitative PCR (RTqPCR) analyses
- Immunoblotting analyses
- TGFβ1 and TGFβ2 ELISA
- In vitro bacterial killing assay
- Sample preparation for RNA-seq
- SMART-seg2
- O Transcript alignment, quantification and filtering
- SMART-seq2 and IPA analyses
- QUANTIFICATION AND STATISTICAL ANALYSIS
- DATA AND SOFTWARE AVAILABILITY

SUPPLEMENTAL INFORMATION

Supplemental Information includes seven figures and two tables and can be found with this article online at https://doi.org/10.1016/j.immuni.2018.11.003.

ACKNOWLEDGMENTS

This work was supported by NIH grant R01-AR069653 to L.Z. and R.L.G. and NIH grants R01-Al083358, R01-AR052728, and U19-Al117673 to R.L.G. M.V.P. is supported by a Pew Charitable Trust grant, NIH grants U01-AR073159 and R01-AR067273, National Science Foundation (NSF) grant DMS1763272, and Simons Foundation grant 594598 (to Qing Nie). C.F.G.J. is supported by NSF-GRFP grant DGE-1321846 and MBRS-IMSD training grant GM055246. Y.Z. is supported by NIH grant R01-Al107027. We thank the flow-cytometry core at the University of California, San Diego, for flow-cytometry studies and Prof. Pier Lorenzo Puri for comments on the manuscript.

AUTHOR CONTRIBUTIONS

L.Z. performed experiments, interpreted data, co-directed the study, and wrote the manuscript. S.C., F.L., and M.L. provided experimental assistance for primary culture and *in vitro* assays and *in vivo* mouse skin infection studies. C.F.G-J performed SMART-seq2, transcript alignment, quantification, filtering, and analyses and revised the manuscript. L.Y. and T.H. provided healthy adult human biopsies from the dermatology clinics at the University of California, San Diego, and C.Y., H.C., and M.L. provided healthy human skin biopsies from dermatology clinics in China. Y.L. and Y.Z. performed flow-cytometry analyses of dermal myeloid immune cells. M.V.P. provided reagents and expertise related to RNA sequencing and revised the manuscript. R.L.G. interpreted data, directed the studies, and wrote the manuscript.

DECLARATION OF INTERESTS

R.L.G. serves on the scientific advisory board and is a consultant for Sente and MatriSys Bioscience and has equity interest.

Received: June 15, 2018 Revised: September 20, 2018 Accepted: November 2, 2018 Published: December 26, 2018

REFERENCES

Bommireddy, R., and Doetschman, T. (2007). TGFbeta1 and Treg cells: alliance for tolerance. Trends Mol. Med. 13, 492–501.

Border, W.A., Noble, N.A., Yamamoto, T., Harper, J.R., Yamaguchi, Yu., Pierschbacher, M.D., and Ruoslahti, E. (1992). Natural inhibitor of transforming growth factor-beta protects against scarring in experimental kidney disease. Nature *360*, 361–364.

Chia, J.J., Zhu, T., Chyou, S., Dasoveanu, D.C., Carballo, C., Tian, S., Magro, C.M., Rodeo, S., Spiera, R.F., Ruddle, N.H., et al. (2016). Dendritic cells maintain dermal adipose-derived stromal cells in skin fibrosis. J. Clin. Invest. *126*, 4331–4345.

Choy, L., and Derynck, R. (2003). Transforming growth factor-beta inhibits adipocyte differentiation by Smad3 interacting with CCAAT/enhancer-binding protein (C/EBP) and repressing C/EBP transactivation function. J. Biol. Chem. 278, 9609–9619.

Dillen, C.A., Pinsker, B.L., Marusina, A.I., Merleev, A.A., Farber, O.N., Liu, H., Archer, N.K., Lee, D.B., Wang, Y., Ortines, R.V., et al. (2018). Clonally expanded $\gamma\delta$ T cells protect against Staphylococcus aureus skin reinfection. J. Clin. Invest. *128*, 1026–1042.

Driskell, R.R., Lichtenberger, B.M., Hoste, E., Kretzschmar, K., Simons, B.D., Charalambous, M., Ferron, S.R., Herault, Y., Pavlovic, G., Ferguson-Smith, A.C., and Watt, F.M. (2013). Distinct fibroblast lineages determine dermal architecture in skin development and repair. Nature *504*, 277–281.

El Agha, E., Moiseenko, A., Kheirollahi, V., De Langhe, S., Crnkovic, S., Kwapiszewska, G., Szibor, M., Kosanovic, D., Schwind, F., Schermuly, R.T., et al. (2017). Two-way conversion between lipogenic and myogenic fibroblastic phenotypes marks the progression and resolution of lung fibrosis. Cell Stem Cell 20. 571.

Festa, E., Fretz, J., Berry, R., Schmidt, B., Rodeheffer, M., Horowitz, M., and Horsley, V. (2011). Adipocyte lineage cells contribute to the skin stem cell niche to drive hair cycling. Cell *146*, 761–771.

Feuerstein, R., Seidl, M., Prinz, M., and Henneke, P. (2015). MyD88 in macrophages is critical for abscess resolution in staphylococcal skin infection. J. Immunol. *194*, 2735–2745.

Futata, E.A., Fusaro, A.E., de Brito, C.A., and Sato, M.N. (2012). The neonatal immune system: immunomodulation of infections in early life. Expert Rev. Anti Infect. Ther. *10*, 289–298.

Georgountzou, A., and Papadopoulos, N.G. (2017). Postnatal innate immune development: from birth to adulthood. Front. Immunol. 8, 957.

Gregoire, F.M., Smas, C.M., and Sul, H.S. (1998). Understanding adipocyte differentiation. Physiol. Rev. 78, 783–809.

Hibino, T., and Nishiyama, T. (2004). Role of TGF-beta2 in the human hair cycle. J. Dermatol. Sci. 35, 9–18.

Hinz, B., Phan, S.H., Thannickal, V.J., Prunotto, M., Desmoulière, A., Varga, J., De Wever, O., Mareel, M., and Gabbiani, G. (2012). Recent developments in myofibroblast biology: paradigms for connective tissue remodeling. Am. J. Pathol. *180*, 1340–1355.

Inman, G.J., Nicolás, F.J., Callahan, J.F., Harling, J.D., Gaster, L.M., Reith, A.D., Laping, N.J., and Hill, C.S. (2002). SB-431542 is a potent and specific inhibitor of transforming growth factor-beta superfamily type I activin receptor-like kinase (ALK) receptors ALK4, ALK5, and ALK7. Mol. Pharmacol. 62, 65–74.

Jinnin, M., Ihn, H., and Tamaki, K. (2006). Characterization of SIS3, a novel specific inhibitor of Smad3, and its effect on transforming growth factor-beta1-induced extracellular matrix expression. Mol. Pharmacol. 69, 597–607.

Kasza, I., Suh, Y., Wollny, D., Clark, R.J., Roopra, A., Colman, R.J., MacDougald, O.A., Shedd, T.A., Nelson, D.W., Yen, M.I., et al. (2014). Syndecan-1 is required to maintain intradermal fat and prevent cold stress. PLoS Genet. *10*, e1004514.

Keophiphath, M., Achard, V., Henegar, C., Rouault, C., Clément, K., and Lacasa, D. (2009). Macrophage-secreted factors promote a profibrotic phenotype in human preadipocytes. Mol. Endocrinol. 23, 11–24.

Kirkland, J.L., Hollenberg, C.H., and Gillon, W.S. (1993). Ageing, differentiation, and gene expression in rat epididymal preadipocytes. Biochimie et biologie cellulaire. 71, 556-561.

Klein, E., Smith, D.L., and Laxminarayan, R. (2007). Hospitalizations and deaths caused by methicillin-resistant Staphylococcus aureus, United States, 1999-2005. Emerg. Infect. Dis. 13, 1840-1846.

Lakos, G., Takagawa, S., Chen, S.J., Ferreira, A.M., Han, G., Masuda, K., Wang, X.J., DiPietro, L.A., and Varga, J. (2004). Targeted disruption of TGFbeta/Smad3 signaling modulates skin fibrosis in a mouse model of scleroderma. Am. J. Pathol. 165, 203-217.

Lee, C.H., Shah, B., Moioli, E.K., and Mao, J.J. (2010). CTGF directs fibroblast differentiation from human mesenchymal stem/stromal cells and defines connective tissue healing in a rodent injury model. J. Clin. Invest. 120, 3340-3349.

Marangoni, R.G., Korman, B.D., Wei, J., Wood, T.A., Graham, L.V., Whitfield, M.L., Scherer, P.E., Tourtellotte, W.G., and Varga, J. (2015). Myofibroblasts in murine cutaneous fibrosis originate from adiponectin-positive intradermal progenitors. Arthritis Rheumatol. 67, 1062-1073.

Miller, L.S., and Cho, J.S. (2011). Immunity against Staphylococcus aureus cutaneous infections. Nat. Rev. Immunol. 11, 505-518.

Miller, L.S., O'Connell, R.M., Gutierrez, M.A., Pietras, E.M., Shahangian, A., Gross, C.E., Thirumala, A., Cheung, A.L., Cheng, G., and Modlin, R.L. (2006). MyD88 mediates neutrophil recruitment initiated by IL-1R but not TLR2 activation in immunity against Staphylococcus aureus. Immunity 24, 79-91.

Mordasky Markell, L., Pérez-Lorenzo, R., Masiuk, K.E., Kennett, M.J., and Glick, A.B. (2010). Use of a TGFbeta type I receptor inhibitor in mouse skin carcinogenesis reveals a dual role for TGFbeta signaling in tumor promotion and progression. Carcinogenesis 31, 2127-2135.

Philippeos, C., Telerman, S.B., Oulès, B., Pisco, A.O., Shaw, T.J., Elgueta, R., Lombardi, G., Driskell, R.R., Soldin, M., Lynch, M.D., and Watt, F.M. (2018). Spatial and single-cell transcriptional profiling identifies functionally distinct human dermal fibroblast subpopulations. J. Invest. Dermatol. 138, 811-825.

Plikus, M.V., Guerrero-Juarez, C.F., Ito, M., Li, Y.R., Dedhia, P.H., Zheng, Y., Shao, M., Gay, D.L., Ramos, R., Hsi, T.C., et al. (2017). Regeneration of fat cells from myofibroblasts during wound healing. Science 355, 748-752.

Rivera-Gonzalez, G.C., Shook, B.A., Andrae, J., Holtrup, B., Bollag, K., Betsholtz, C., Rodeheffer, M.S., and Horsley, V. (2016). Skin adipocyte stem cell self-renewal is regulated by a PDGFA/AKT-signaling axis. Cell Stem Cell 19 738-751

Schmidt, B.A., and Horsley, V. (2013). Intradermal adipocytes mediate fibroblast recruitment during skin wound healing. Development 140, 1517-1527.

Shaw, A.C., Goldstein, D.R., and Montgomery, R.R. (2013). Age-dependent dysregulation of innate immunity. Nat. Rev. Immunol. 13, 875-887.

Soma, T., Tsuji, Y., and Hibino, T. (2002). Involvement of transforming growth factor-beta2 in catagen induction during the human hair cycle. J. Invest. Dermatol. 118, 993-997.

Sun, K., Tordjman, J., Clément, K., and Scherer, P.E. (2013). Fibrosis and adipose tissue dysfunction. Cell Metab. 18, 470-477.

Tabib, T., Morse, C., Wang, T., Chen, W., and Lafyatis, R. (2018). SFRP2/DPP4 and FMO1/LSP1 define major fibroblast populations in human skin. J. Invest. Dermatol. 138, 802-810.

Zhang, L.J., Guerrero-Juarez, C.F., Hata, T., Bapat, S.P., Ramos, R., Plikus, M.V., and Gallo, R.L. (2015). Innate immunity. Dermal adipocytes protect against invasive Staphylococcus aureus skin infection. Science 347, 67-71.

Zhang, L.J., Sen, G.L., Ward, N.L., Johnston, A., Chun, K., Chen, Y., Adase, C., Sanford, J.A., Gao, N., Chensee, M., et al. (2016). Antimicrobial peptide LL37 and MAVS signaling drive interferon-β production by epidermal keratinocytes during skin injury. Immunity 45, 119-130.

Zwick, R.K., Guerrero-Juarez, C.F., Horsley, V., and Plikus, M.V. (2018). Anatomical, physiological, and functional diversity of adipose tissue. Cell Metab. 27, 68-83.

STAR***METHODS**

KEY RESOURCES TABLE

REAGENT or RESOURCE	SOURCE	IDENTIFIER
Antibodies		
Rabbit anti-CRAMP	University of California San Diego	Dr. Richard Gallo
Rabbit anti-LL37	University of California San Diego	Dr. Richard Gallo
goat anti-COLIV	Millipore	Cat# AB769; RRID: AB_92262
Mouse anti-FABP4	Abcam	Cat# ab188387
Rabbit anti-Phospho-SMAD2, 3	Cell Signaling	Cat# 8828; RRID: AB_2631089
Rabbit anti-SMAD2/3	Abcam	Cat# ab202445
rabbit anti-phospho-AKT antibody	Cell Signaling	Cat# 4060; RRID: AB_2315049
mouse anti-AKT	Cell Signaling	Cat# 4691; RRID: AB_915783
anti-mouse CD16/32	eBioscience	Cat# 14016185; RRID: AB_467134
PECy7 anti-CD45	BioLegend	Cat# 147704; RRID: AB_2563536
PerCP-Cy5.5 anti-CD31	BioLegend	Cat# 102522; RRID: AB_2566761
PE anti-THY1	BioLegend	Cat# 105308; RRID: AB_313179
APC anti-PDGFRA	eBioscience	Cat# 17140181; RRID: AB_529482
BV605 anti-Sca1	BioLegend	Cat# 108133; RRID: AB_2562275
AF488 anti-SMA	eBioscience	Cat# 53976082; RRID: AB_2574461
APC anti-CD4	Biolegend	Cat# 100516; RRID: AB_312719
BV510 anti-CD8a	Biolegend	Cat# 100752; RRID: AB_2563057
APC-Cy7 anti-TCRβ	Biolegend	Cat# 109220; RRID: AB_893624
PE anti-TCRδγ	eBioscience	Cat# 12571182; RRID: AB_465934
PerCP-Cy5.5 anti-CD45.2	Biolegend	Cat# 109828; RRID: AB_893350
PECy7 anti-CD11B	Biolegend	Cat# 101216; RRID: AB_312799
FITC anti-Ly6G	eBioscience	Cat# 11593182; RRID: AB_465314
PE anti-F4/80	eBioscience	Cat# 12480182; RRID: AB_465923
APC anti-CD11C	Biolegend	Cat# 117310; RRID: AB_313779
AF700 anti-MHCII	eBioscience	Cat# 56-5321-82; RRID: AB_494009
zombie violet viability dye	Biolegend	423114
Bodipy	ThermoFisher Scientific	D3922
Bacterial and Virus Strains		
S. aureus USA300	University of California San Diego	Dr. Victor Nizet
S. aureus SA113	University of California San Diego	Dr. Victor Nizet
Biological Samples		
Mouse skin, spleen, blood samples	University of California San Diego, Animal Facility	N/A
Neonatal human skin samples	International Institute for Advancement of Medicine (IIAM)	N/A
Adult human skin samples	University of California San Diego, Dermatology clinics	N/A
Chemicals, Peptides, and Recombinant Pro		
SB431542	Selleckchem	S1067
SIS3	Selleckchem	S7959
Wortmannin	EMD Millipore	9951
3-Isobutyl-1-methylxanthine (IBMX)	SIGMA-ALDRICH	15879
Indomethacin	SIGMA-ALDRICH	18280
Dexamethasone	SIGMA-ALDRICH	D4902
		(Continued on next page

(Continued on next page)

Continued		
REAGENT or RESOURCE	SOURCE	IDENTIFIER
Insulin	SIGMA-ALDRICH	91077C
DMEM, high glucose	Thermo Fisher Scientific (Life Technologies)	11965118
Antibiotic-Antimycotic	Thermo Fisher Scientific (Life Technologies)	15240062
Glutamax	Thermo Fisher Scientific (Life Technologies)	35050-061
Recombinant mouse TGFβ1	R&D Systems	7666-MB-005
Recombinant mouse TGFβ2	R&D Systems	7346-B2-005
PureLink RNA Mini Kit	Thermo Fisher Scientific (Life Technologies)	12183025
Collagenase D from Clostridium histolyticum	Roche	11088882001
Deoxyribonuclease I from bovine pancreas, Type IV, lyophilized powder	SIGMA-ALDRICH	D5025-150KU
RNase-free DNase Set	QIAGEN	79254
iScript cDNA synthesis kit	Bio-Rad	1725038
2x SYBR Green qPCR Master Mix	Bimake	B21202
Super Script II Reverse Transcriptase	Invitrogen	18064014
KAPA HiFi Hotstart ReadyMix	Kapa Biosystems	KK2601
AMPure XP beads	Beckman Coulter	A63881
Critical Commercial Assays		
Gomori Trichrome green collagen staining kit	ThermoFisher Scientific	87021
Hydroxyproline assay kit	BioVision	K555-100
Mouse TGF-beta 1 ELISA	R&D Systems	DY7346-05
Mouse TGF-beta 2 ELISA	R&D Systems	DY7346-05
Intracellular Fixation & Permeabilization	eBioscience	88-8824-00
Buffer Set		
Nextera DNA Sample Preparation kit	Illumina	FC-121-1030
NextSeq 500 High Output Kit v2 – 75 cycles	Illumina	FC-404-2005
Deposited Data		
RNA-seq data of cultured E14 ~2 month dermal fibroblasts	NCBI Gene Expression Omnibus (GEO)	GEO: GSE121460
Experimental Models: Cell Lines		
Primary mouse or human dermal fibroblasts	This study	Isolated from mouse or human skin dermis
Experimental Models: Organisms/Strains		
Camp ^{flox/flox} mice	This study	Dr. Richard Gallo
Pdgfra-cre mice	Jackson laboratory	013148
Adipoq-cre mice	Jackson laboratory	028020
Tgfbr2 ^{flox/flox}	Jackson laboratory	012603
Oligonucleotides	·	
Mouse primers for RTqPCR	Integrated DNA Technologies (IDT)	See Table S1 for primer sequences
Human primers for RTqPCR	Integrated DNA Technologies (IDT)	See Table S2 for primer sequences
Software and Algorithms	5 , ,	
GraphPad Prism	GraphPad Software, Inc.	N/A
FlowJo V10	FlowJo LLC	N/A
Ingenuity pathway analysis	QIAGEN	N/A
Bowtie		http://bowtie-bio.sourceforge.net/
		manual.shtml
RSEM		https://github.com/deweylab/RSEM
Next maSigPro		https://www.bioconductor.org/packages/
		release/bioc/html/maSigPro.html

CONTACT FOR REAGENT AND RESOURCE SHARING

Further information and requests for resources and reagents should be directed to and will be fulfilled by the Lead Contact, Richard L. Gallo (rgallo@ucsd.edu).

EXPERIMENTAL MODEL AND SUBJECT DETAILS

Animals and animal care

All animal experiments were approved by the University of California, San Diego (UCSD), Institutional Animal Care and Use committee. C57BL/6 wild-type mice were originally purchased from Jackson laboratory, and were then breeded and maintained in animal facility of UCSD. For aging mouse model, dorsal skin biopsies were collected from C57BL/6 wild-type male mice with various ages (E14, P1, 3W, 2 months and 1 year old). *Pdgfra-cre* mice (Stock No: 013148), *Adipoq-cre* mice (Stock No: 028020) and *Tgfbr2*^{flox/flox} mice (Stock No: 012603) were originally purchased from Jackson laboratory then breeded and maintained in animal facility of UCSD. *Camp*^{flox/flox} mice, in which exon 2 and exon 4 of Camp gene were flanked by LoxP sites, were generated by Ozgene (Bentley DC, WA, Australia) Fibroblasts or adipocyte specific deletion of *Camp* were generated by breeding *Camp*^{flox/flox} mice with *Pdgfra-cre* mice or *Adipoq-cre* mice respectively. *Tgfbr2* specific deletion in fibroblasts was achieved by breeding *Tgfbr2*^{flox/flox} mice with *Pdgfra-cre* mice. Probably due to early embryonic lethality, we were not able to get the homozygous deletion of *Tgfbr2* in fibroblasts (*Tgfbr2*^{flox/flox}; *Pdgfra-cre*) over more than one year of breeding, so the heterozygous deletion of *Tgfbr2* in fibroblasts (*Tgfbr2*^{flox/flox}; *Pdgfra-cre*) was used instead as the *Tgfbr2* heterozygous deletion model to study the role of TGFBR pathway in the infection triggered dermal adipogenesis-antimicrobial response. Dorsal skin biopsies around the same area were collected from mice with various ages for analysis to control the consistency of the tissue site collected over the whole lifetime of the mouse

Mouse model of S. aureus skin infection

Skin infection experiments were done as described before (Zhang et al., 2015). Staphylococcus aureus strain USA300 (MRSA) was used for *in vivo* infection. In brief, the backs of sex-matched and age-matched adult wild-type or indicated strain of mutant mice were shaved and hair removed by chemical depilation (Nair) then injected subcutaneously with 100 μ L of a mid-logarithmic growth phase of S. aureus (1x 10⁷ CFU of bacteria) in PBS. Mice were sacrificed after day 3 and skin biopsy covering the infection area was harvested. Skin biopsies were homogenized in 1 mL Trizol (for RNA) or PBS (for CFU counting) with 2 mm zirconia beads in a mini-bead beater 16 (Biospect, Bartlesville, OK). To count CFU, homogenized skin samples were serially diluted, plated onto Tryptic Soy Agar, and enumerated after 18 hr to quantify the CFU per gram of tissue. For administration of TGFBR inhibitor, SB431542 (0.125 mg in 100uL of 2% DMSO + 30% PEG300 + PBS) or vehicle control was injected intradermally within the infection site at 24 hr and 48 hr post infection and skin biopsies were collected at day 3 post infection for RNA extraction or CFU count as described above. For all animal studies, animals were randomly selected without formal pre-randomization and quantitative measurements were done without the opportunity for bias.

METHOD DETAILS

Chemicals, antibodies and dyes

IBMX (3-Isobutyl-1-methylxanthine), dexamethasone, indomethacin, and recombinant human insulin were purchased from Sigma-Aldaich (St. Louis, MO). SB431542 and SIS3 were purchased from Selleckchem (Houston, TX). Wortmannin was purchased from EMD Millipore (Billerica, MA). Rabbit anti-CRAMP and rabbit anti-LL-37 antibodies were made from our lab as described previously (Zhang et al., 2015; Zhang et al., 2016); goat anti-COLIV, mouse anti-FABP4 and rabbit anti-SMAD2/3 antibodies are from Abcam (Cambridge, MA); Lipid dye bodipy is from Molecular Probes (Eugene, OR). Rabbit anti-Phospho-SMAD2, 3, rabbit anti-phospho-AKT antibody and mouse anti-AKT antibody were purchased from Cell Signaling (Danvers, MA). Recombinant mouse TGFβ1 and TGFβ2 were purchased from R&D Systems (Minneapolis, MN).

Human skin sample collection

Fresh adult human (Caucasian) full thickness skin biopsies, from the back of healthy and non-obese male donors between 18~90 years of age, were collected by the Dermatology clinics, University of California San Diego. Fresh adult human (Chinese) full thickness skin biopsies were collected by Hospital for skin disease, Institute of Dermatology, Chinese Academy of Medical Science and Peking Union Medical College. All sample acquisitions, were approved and regulated by the University of California San Diego Institutional Review Board (reference number 140144) or by Institute of Dermatology, Chinese Academy of Medical Science Medical Ethics Committee (reference number 2012003). The informed consent was obtained from all subjects prior to skin biopsies. Fresh neonatal full thickness skin samples, from the back of neonatal donors, were obtained from the international institute for advancement of Medicine (IIAM; Exton, PA). The informed consent was obtained from parent of neonatal donor prior to skin collection. All human biopsies were taken from the back skin, where it is relatively protected from sun exposure compared to other regions such as face and neck of the body. Upon collection, these samples were directly fixed with PFA then proceed for either paraffin embedding or OCT embedding for histological or immunofluorescent analyses.



Histology, collagen trichrome staining and immunohistochemistry (IHC)

Paraffin embedding and sectioning was performed by the Moores cancer center histology core at UCSD. For OCT embedding, tissue biopsies were first fixed with 4% PFA for 2 hours then cryoprotected by sucrose for 48 hours prior to being embedded in OCT compound and stored in -80° C. Histological analysis was performed using either paraffin sections or frozen sections by Hematoxylin-Eosin (H&E) staining. Collagen was stained by the Richard-Allan Scientific Gomori Trichrome green collagen staining kit (ThermoFisher Scientific, Waltham, MA, USA). Elastic staining (Thermo Fisher Scientific, Waltham, MA, USA) and hydroxyproline assay (BioVision) were performed on human or mouse tissues according to manufacturer's instructions. For IHC, fixed and permeabilized tissue sections were blocked with Image-iT FX reagent (invitrogen) before incubating with primary antibodies followed by appropriate 488- or Cy3-coupled secondary antibodies. Nuclei were counter-stained with DAPI. All images were taken with an Olympus BX41 microscope (widefield) or Zeiss LSM510 confocal microscope as indicated.

Primary dermal fibroblast isolation and culture

For neonatal mouse dorsal skin, epidermis was first removed from the dermis by overnight dispase digestion as described before, and for adult skin hair was first removed by clipper then cut into 5mm wide strips prior to dispase digestion. The dermis was then cut into small pieces (\sim 1 mm) by scalpel then digested with 2.5 mg/mL Collagenase D and 30 ng/mL DNase1 for 2 hours at 37°C with constant rocking to release dermal fibroblasts. Cells mixture was then filtered through 30 μ m filter into single cell suspension then treated with red blood cell lysis buffer. Isolated dermal fibroblasts were cultured in growth medium (DMEM supplemented with 10% FBS, glutamax and antibiotics-antimicotics) in a humidified incubator at 5% CO2 and 37°C under sterile conditions. Fresh medium was replenished daily to remove debris or dead cells. Primary cells were then trypsinized within 3 days and replated at 5 × 10⁴/mL for *in vitro* assays, and only passage 1 cells were used for experiment. To induce adipocyte differentiation, two day post-confluent dFB were switched to adipocyte differentiation medium containing 2 μ M Dexamethasone, 250 μ M IBMX, 200 μ M Indomethacin and 10 μ g/mL recombinant human insulin. Fresh differentiation medium was changed at day 2, 4, and 7 during the differentiation time course.

Flow cytometry and analysis (FACS)

FACS analysis of primary dermal fibroblasts was modified from previously reported method for adipogenic fibroblasts (Chia et al., 2016; Rivera-Gonzalez et al., 2016). Briefly, freshly isolated dFB from mouse skin or primary cultured of dFB first were stained with zombie violet viability dye (BioLegend, 423114) to stain dead cells. Cells were then blocked with anti-mouse CD16/32 (eBioscience, 14016185), followed by staining with an antibody cocktails containing PECy7-CD45 (BioLegend, 147704), PerCP-Cy5.5-CD31 (BioLegend, 102522), PE-THY1 (BioLegend, 105308), APC-PDGFRA (CD140a) (eBioscience, 17140181) and BV605-Sca1 (BioLegend, 108133). Stained cells were then fixed and permeabilized using the intracellular fixation and permeabilization buffer set (eBioscience), then intracellular SMA was stained by AF488-SMA (eBioscience, 53976082). For FACS staining of T cell populations, cells were stained with an antibody cocktail including APC-CD4 (Biolegend, 100516), BV510-CD8a (Biolegend, 100752), APC-Cy7-TCRβ (Biolegend, 12-5711-82), PE-TCRδγ (eBioscience, 12-5711-82), and PerCP-Cy5.5-CD45.2 (Biolegend, 109828). For FACS staining of other myeloid immune cell panel, cells were stained with an antibody cocktail including PECy7-CD11B (BioLegend, 101216), FITC-Ly6G (eBioscience, 11593182), PE-F4/80 (eBioscience, 12480182), APC-CD11C (BioLegend, 117310), AF700-MHCII and (eBioscience, 56532182) FACS analysis for protein expression of each cell marker was performed by the BD FACSCanto RUO machine and analyzed by FlowJo V10 software. Dead cells stained positive with zombie violet dye were excluded from the analyses.

Reverse transcription-quantitative PCR (RTqPCR) analyses

Total cellular RNA was extracted using the PureLink RNA isolation kit with RNase-free DNase1 digestion to remove genomic DNA contamination (QIAGEN) and 500 ng of RNA was reverse transcribed to cDNA using iScript cDNA synthesis kit (Bio-rad). Quantitative, real-time PCR was performed on the CFX96 real time system (Bio-rad) using SYBR Green Mix (Bimake, Houston, Tx). All of the primers used with SYBR green were designed to span at least one exon to minimize the possibility of nonspecific amplification from the genomic DNA. The expression of *Tbp* gene (TATA-Box Binding Protein) was used as a house keeping gene to normalize data for the expression of mouse genes, and *HPRT* was used as a house keeping gene for the expression of human genes. Specific primer sequences are shown in Table S1 (mouse genes) and Table S2 (human genes).

Immunoblotting analyses

10ul of cell medium was separated on a 10%–20% Tris-Tricine precast gel (Biorad), transferred to PVDF membrane (Biorad), followed by immunoblotting using indicated primary antibodies followed by fluorescent secondary antibodies (LICOR) and imaging using fluorescent Odyssey System (LICOR).

TGFβ1 and TGFβ2 ELISA

Mouse TGFβ1 or TGFβ2 ELISA Kit was purchased from R&D Systems (Minneapolis, MN) and TGFβ1 orTGFβ2 concentrations in conditioned medium from primary mouse dermal fibroblasts or mouse serum were determined according to manufacturer's instruction.

In vitro bacterial killing assay

Antibiotic free and phenol-red free conditioned medium was collected from differentiating dermal fibroblasts as described before (Zhang et al., 2015). The conditioned medium (100 μL) was then mixed with 10⁵/ml CFU (colony forming unit) of indicated bacterial strain in 96 well tissue culture microtiter plates and incubated at 37°C for 10 ~48 hr prior to plating for CFU counting. The optical density at 595 nm (OD595) was also measured every 2~4 hours by a spectrometer.

Sample preparation for RNA-seq

Primary dermal fibroblasts, isolated from dorsal skin of mouse at E14, E17, P1, 3 weeks and 2 months of age, were harvested at the first passage. To enrich fibroblasts that have committed to adipocyte lineage, Sca1+ dFB were purified from P1, 3 week and 2 month dFB using the anti-Sca1 microbeads kit and MACS columns and separators (Miltenyi Biotec, San Diego, CA). Purity of cells from each age group was greater than 90% as confirmed by FACS analyses. Total cellular RNA was extracted using the PureLink RNA isolation kit with DNase1 digestion to remove genomic DNA contamination (Life Technologies) and 10 ng total RNA (n = 3 for each age group) was used for SMART-seq2.

SMART-seq2

SMART-seg2 was performed as previously described with minor. Briefly, 10 ng total RNA (RIN > 9.6) was reversed transcribed using Super Script II (Invitrogen). cDNA was pre-amplified for 10 cycles using high fidelity KAPA HiFi HotStart Ready Mix (Kapa Biosystems). Pre-amplified cDNAs were cleaned with AMPure XP beads (Beckman Coulter) at a 1:1 ratio and eluted with elution buffer (QIAGEN). Tn5-mediated tagmentation was performed on 18 ng total cDNA using the Nextera DNA Sample Preparation Kit (Illumina) at 55°C for 5 minutes and deactivated with PM buffer (QIAGEN). Adaptor-ligated fragments were amplified for 8 continuous cycles using universal Ad1 and unique Ad2.xx barcodes (IDT). Amplified PCR fragments were purified with AMPure XP beads as suggested (Beckman Coulter). Size selected libraries were quantified using Qubit (Thermo), loaded on a High-Sensitivity DNA chip for quality control (Agilent), and quantified using KAPA for Illumina Sequencing Platforms (Illumina). Libraries were multiplexed and sequenced as paired-end, 43 bps on a NextSeq 500 Illumina Sequencing Platform (Illumina) (Cluster density = 252K/mm2, Clusters PF = 78.8%, Q30 = 90.7%).

Transcript alignment, quantification and filtering

Paired-end reads were aligned to the mouse genome (mm10/gencode.vM4) with bowtie (version 1.0.0) and quantified using the RNAseq by Expectation-Maximization algorithm (RSEM) (version 1.2.12) with the following standard parameters: rsem-calculate-expression -p \$CORES-paired-end. Samples displaying > 12,000,000 aligned reads and > 77% alignment were considered for downstream analyses. Samples were filtered and only protein-coding genes and IncRNAs expressed at minimum 1 TPM in at least one sample in all biological replicates were considered for downstream analyses.

SMART-seq2 and IPA analyses

Differential expression dynamics across E14, E17, P1-Sca1+, 3W-Sca1+, 2M-Sca1+ samples was identified using the single-time series, two-step regression model algorithm Next maSigPro using with the following parameters under the T.Fit, get.siggenes and see genes functions: alfa = 0.01, vars = "all," rsq = 0.7, k = 7. Principle component analyses were performed using the R ggbiplot package. Pathway and upstream regulator analyses were performed by Ingenuity pathway analysis (IPA) from QIAGEN.

QUANTIFICATION AND STATISTICAL ANALYSIS

Experiments were repeated at least 3 times with similar results. Statistical significance was determined using Student's unpaired two-tailed t test, or one way ANOVA multiple comparison test as indicated in the legend (*p < 0.05, **p < 0.01, ***p < 0.001, ****p < 0.0001).

DATA AND SOFTWARE AVAILABILITY

RNA-seq data of cultured dermal fibroblasts reported in this paper has been deposited to NCBI Gene Expression Omnibus (GEO), GEO: GSE121460.